Available online at www.sciencedirect.com
SCIENCE DIRECT
ELSEVIER
Coordination Chemistry Reviews 249 (2005) 2880–2908
COORDINATION CHEMISTRY REVIEWS
www.elsevier.com/locate/ccr

Review

The synthesis and coordination chemistry of 2,6-bis(pyrazolyl)pyridines and related ligands — Versatile terpyridine analogues

Malcolm A. Halcrow *

School of Chemistry, University of Leeds, Woodhouse Lane, Leeds LS2 9JT, UK

Received 21 November 2004; accepted 10 March 2005
Available online 19 April 2005

Contents

Abstract

Derivatives of 2,6-di(pyrazol-1-yl)pyridine and 2,6-di(pyrazol-3-yl)pyridine have been used as ligands for 15 years, and have both advantages and disadvantages in this regard compared to the much more widely investigated terpyridines. A review of the synthesis of these and some

Abbreviations: acacH, 2,4-pentanedione; bipy, 2,2′-bipyridine; cod, 1,5-cyclooctadiene; dcbipy, 2,2′-bipyridine-4,4′-dicarboxylic acid; dmf, dimethylformamide; DF, density functional; dmso, dimethylsulfoxide; e.e., enantiomeric excess; Me_2bipy, 4,4′-dimethyl-2,2′-bipyridine; MV^{2+}, methylviologen, *N*,*N*′-dimethyl-4,4′-bipyridinium; phen, 1,10-phenanthroline; pic, picrate ($[2,4,6\text{-}(NO_2)_3C_6H_2O]^-$); PPN, bis(triphenylphosphoranylidene)ammonium ($[PhP_3{=}N{=}PPh_3]^+$); QM/MM, quantum mechanics/molecular mechanics; Tf^-, trifluoromethanesulfonate ($CF_3SO_3^-$); thf, tetrahydrofuran; Ts^-, tosylate ($[CH_3C_6H_4SO_3\text{-}4]^-$); ttpy, 4′-(4-methylphenyl)-2,2′:6′,2″-terpyridine

* Tel.: +44 113 343 6506; fax: +44 113 343 6565.
E-mail address: M.A.Halcrow@chem.leeds.ac.uk.

doi:10.1016/j.ccr.2005.03.010

related ligand types, and a survey of their complex chemistry, are presented. Highlights of the latter include luminescent lanthanide compounds for biological sensing, and iron complexes showing unusual thermal and photochemical spin-state transitions.

Keywords: Tridentate ligands; Synthesis; Lanthanide complexes; Spin-crossover

1. Introduction

2,2′:6′,2″-Terpyridine (terpy) and its derivatives form one of the most widely studied classes of ligands in coordination chemistry [1]. The popularity of terpy as a ligand is easy to understand. It is commercially available and straightforward to synthesise, while several types of derivatised terpy, particularly those substituted at the 4′-position, are also readily accessible [2]. Terpy can bind to both low- and high-oxidation state metal ions, almost always in tridentate fashion [1,3] (although bidentate and monodentate coordination of terpy derivatives to the monovalent coinage metals is common [4]). As with other polypyridyl ligands, terpyridine complexes can have novel redox chemistries involving ligand radical products, and those of the late second and third row elements are often strongly luminescent [5,6]. This property, and the synthetic accessibility of substituted terpys, have also led to metal-bis(terpy) centres being incorporated into coordination polymers, dendrimers, and other functional supramolecular structures [7].

This article discusses the synthesis and coordination chemistry of the 2,6-di(pyrazolyl)pyridine family of triden-

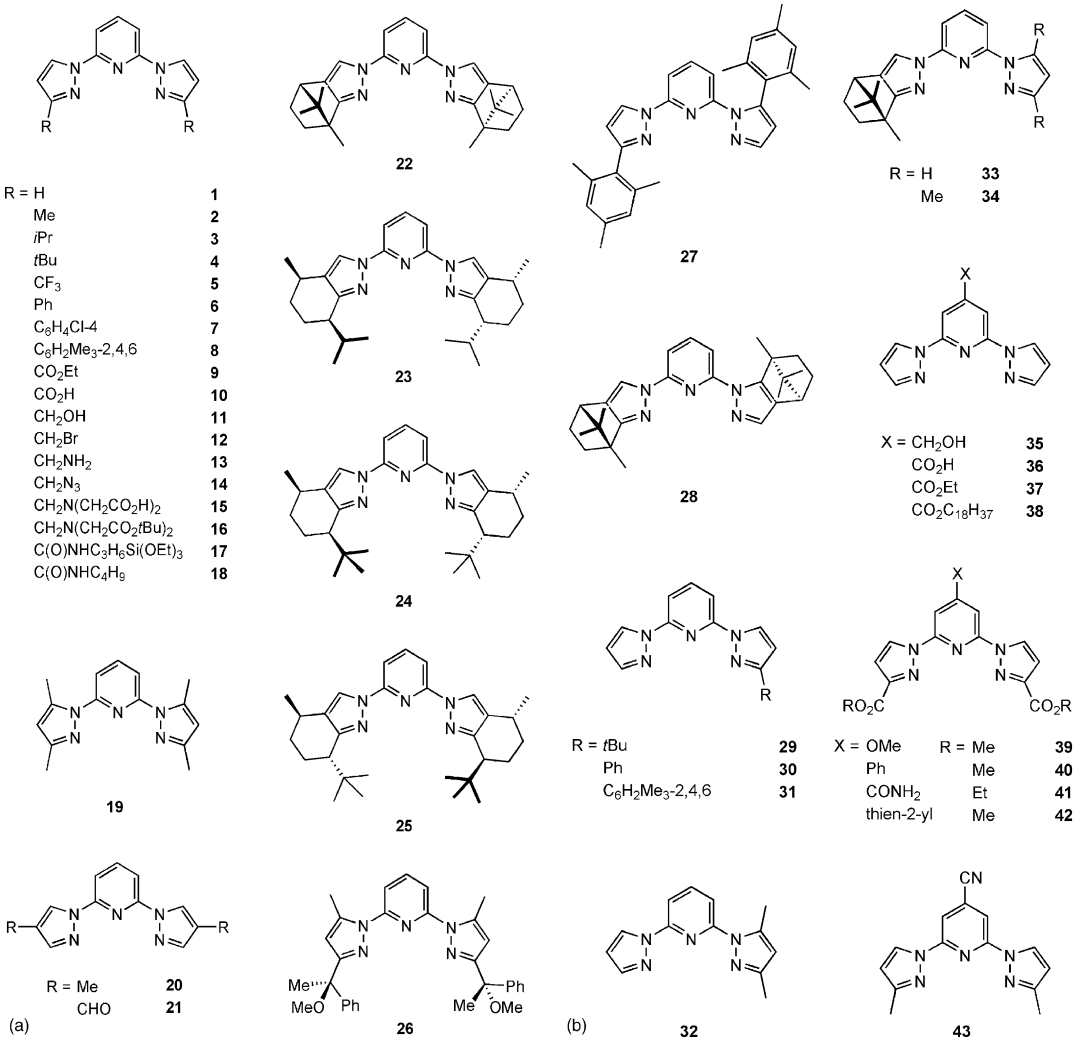

Scheme 1. Ligands referred to in this study.

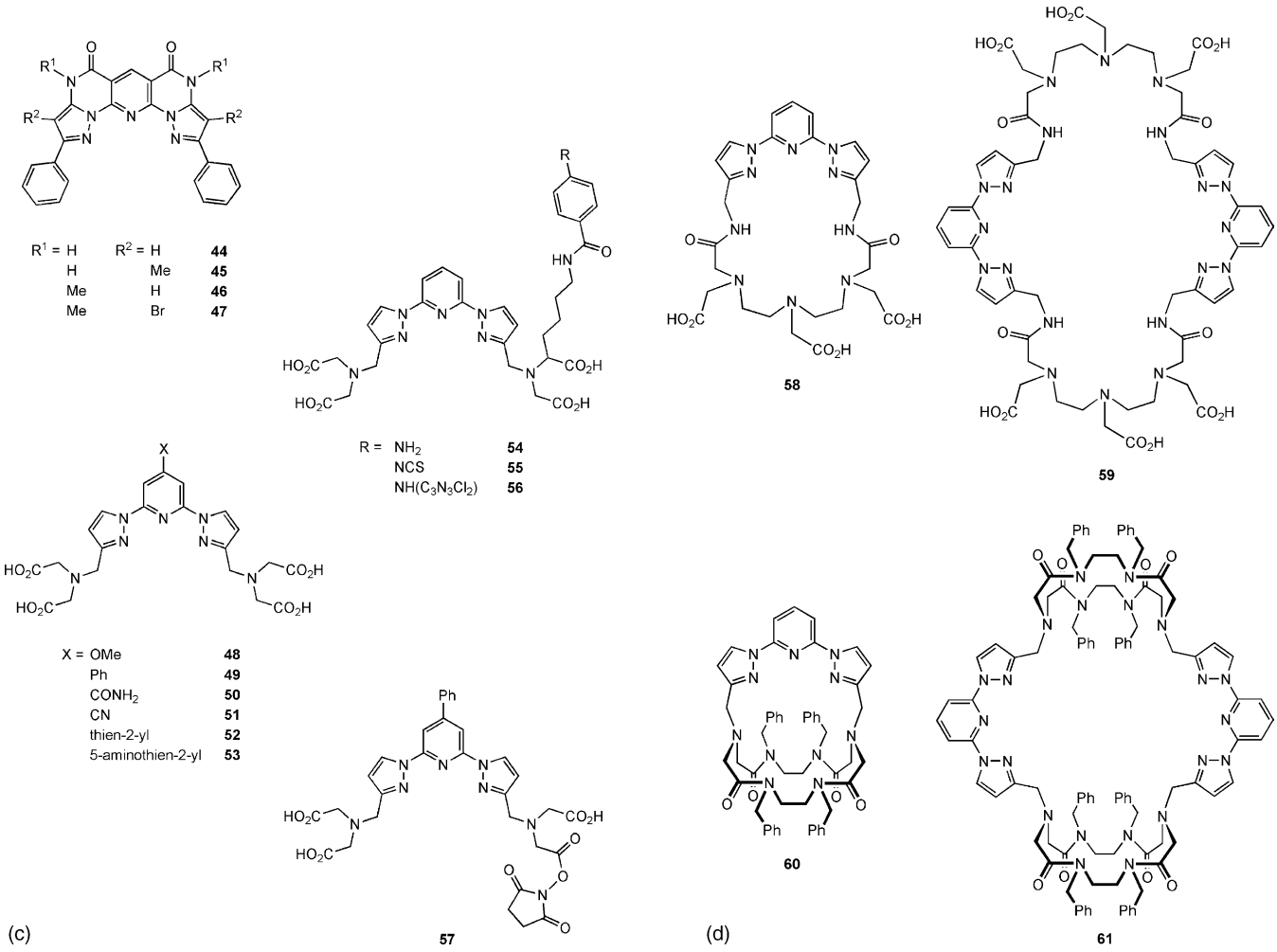

Scheme 1. (*Continued*)

tate ligands. Despite their superficial similarity, the chemistry of these ligands differs from terpyridine chemistry in several important ways. On one hand incorporation of different heterocycles into the ligand framework, with their differing basicities and π-orbital energies, has a substantial effect on the electron richness, kinetic lability and luminescent properties of the resultant metal complexes. On the other, different regioisomers of substituted 2,6-di(pyrazolyl)pyridine derivative are amenable to synthesis compared to the terpyridine system, since the synthetic routes to the two classes of compound are different. Two geometric isomers of the 2,6-di(pyrazolyl)pyridine framework are known, both of which have been widely studied as ligands and are considered in this article. Separate sections will describe the syntheses of each class of 2,6-dipyrazolylpyridine, and their coordination chemistry. Finally the chemistry of three related ligand classes, which have been less studied to date, is also considered. Ligands and complexes in which pyridyl and pyrazolyl moieties are linked by a methylene spacer are outside the scope of this article, but have been reviewed elsewhere [8] (Scheme 1).

2. 2,6-Di(pyrazolyl)pyridine ligand syntheses and structures

2.1. Syntheses and structures of 2,6-di(pyrazol-1-yl)pyridines

The usual method for the preparation of 2,6-di(pyrazol-1-yl)pyridines is the nucleophilic coupling of 2 equiv. of deprotonated pyrazole with 2,6-dibromopyridine (Eq. (1)) [9].

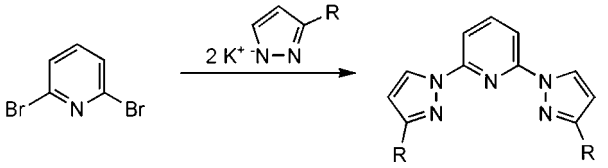

(1)

While dibromopyridine is the most commonly used starting material in this reaction, 2,6-dichloropyridine can also

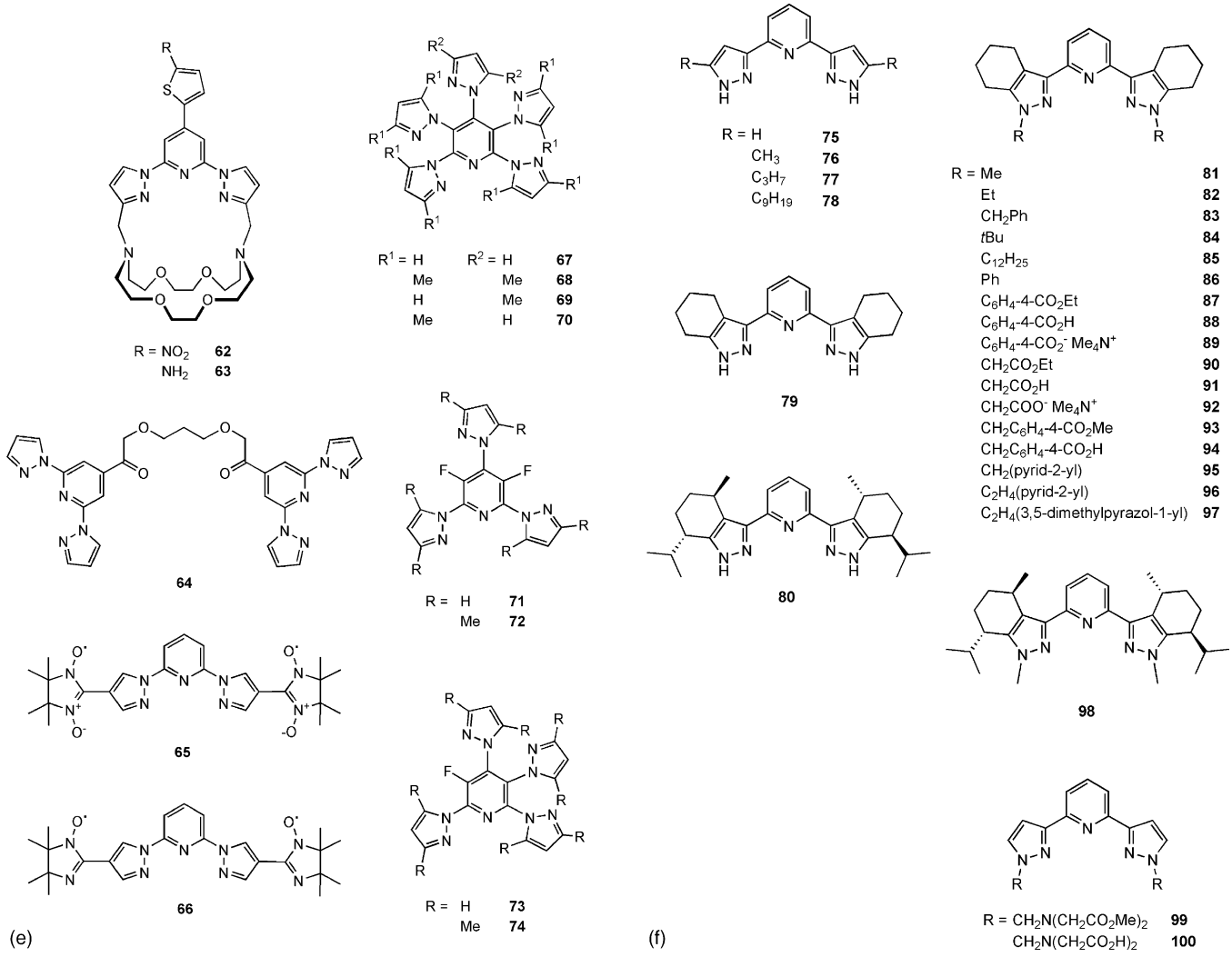

Scheme 1. (*Continued*)

be employed with only a small reduction in yield [9]. The pyrazolide salt is usually generated in situ by treatment of the pyrazole starting material with KH or potassium metal. Easier-to-handle NaH can also give good yields in at least some cases, however [10,11]. This reaction requires quite forcing conditions to drive to completion: an excess of pyrazolide reagent (3 equiv. is typical), a high reaction temperature (130 °C) in a high-boiling solvent such as diglyme, and several days of reaction time are commonly used. However, the product can usually be precipitated from the reaction mixture in yields of 50–70% by simply quenching with excess water (unless it is low-melting, like **3** [12]), and can often be purified by a single recrystallisation.

The following C_2-symmetric ligands have been synthesised through this basic sequence, or by subsequent derivatisation of a preformed 2,6-di(pyrazol-1-yl)pyridine skeleton (see below): **1**, **4**, **6** and **19** [9], **2** and **20** [10], **3** [12], **5** [13], **7** [14], **8** [15], **9**–**12**, **15** and **16** [16], **13** and **14** [17], **17** and **18** [18], **21** [19], **22** [20], **23** [21], the optical isomers **24** and **25** [22], and **26** [23]. The most common impurity in crude preparations of these ligands is the mono-substituted intermediate **I** [16,20]. However, where a 3{5}-substituted pyrazole starting material is used, different regioisomeric products **II**–**IV** can be obtained. Selectivity for the 3,3″-disubstituted product **II** on steric grounds is usually high, although the 3,5″-disubstituted isomer **III** is sometimes a significant byproduct [9,12,20]. Ligands **27** [12] and **28** [20] of type **III** have been purified in 8–12% yield from crude preparations of **8** and **22**, respectively. The relative yields of products **II** and **III** in these two cases imply that ca. 5% of all the nucleophilic substitution events in the reactions led to a 1,5- rather than a 1,3-disubstituted pyrazole moiety. No products of structure **IV** have yet been isolated from these reactions. The monosubstituted species **I** can in fact be purified in ca. 60% yield from reaction (1), by using just 1 equiv. of pyrazolide reagent and by performing the reaction at a lower temperature (ca. 60 °C) and for a shorter time (2 days) [9,20,23]. The second substitution step can then be performed in 45–80% yield using a different pyrazole, under the same more forcing conditions

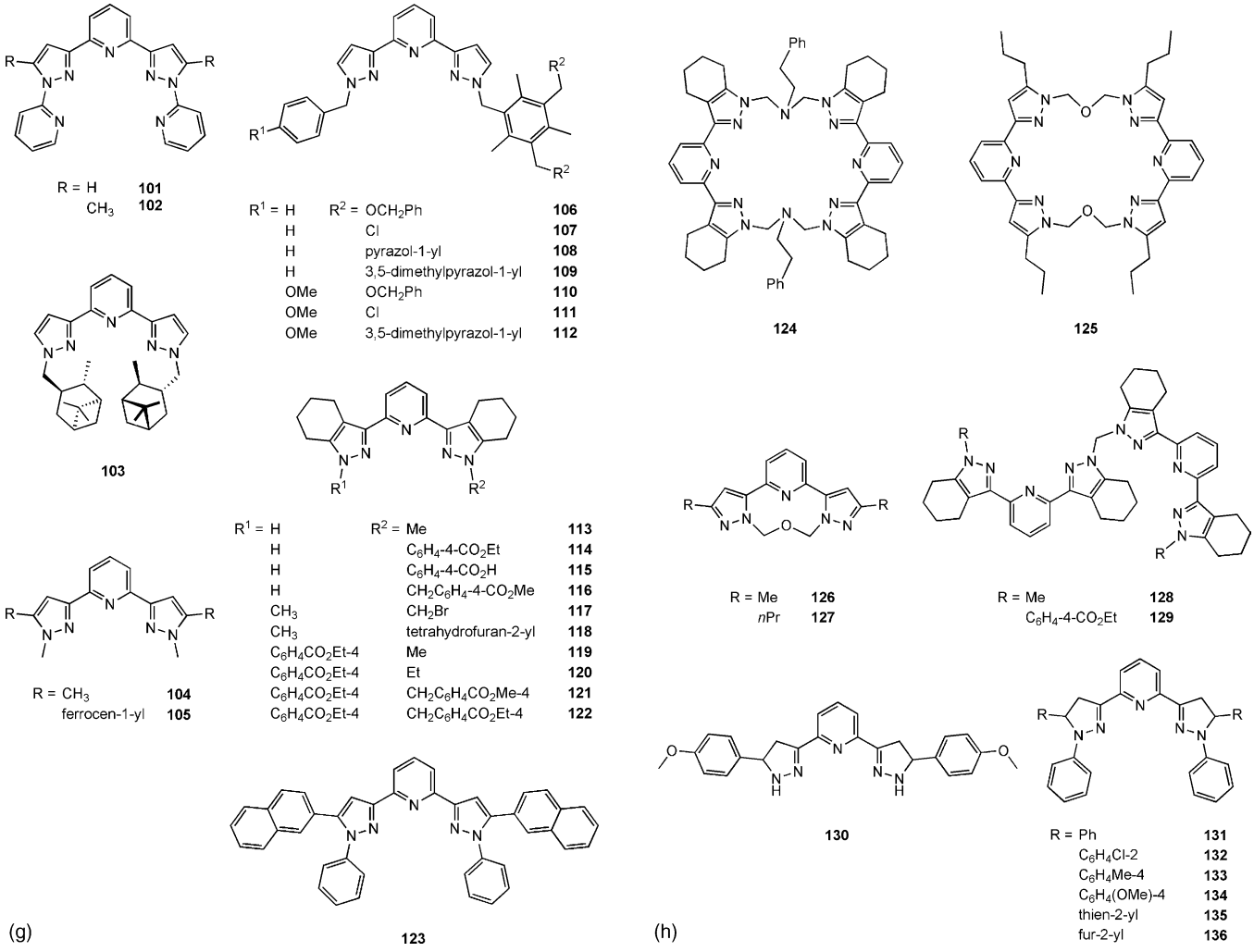

Scheme 1. (*Continued*)

used to make **1**–**26** [9]. In this way, the unsymmetrically substituted ligands **29**, **30** and **32** [9], **31** [24], **33** and **34** [20] have been synthesised.

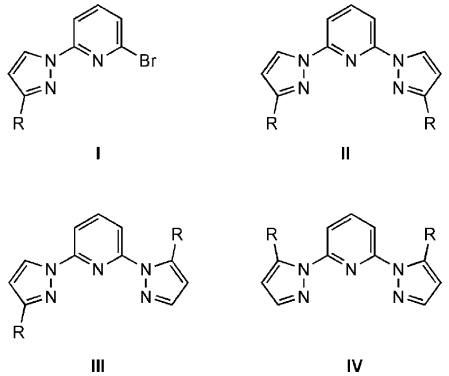

Unfortunately, the success of reaction (1) is rather dependent on substitution at the pyridine ring. For example, the yields of the reactions described in Eq. (2) are 55% (X = H) [16], 10% (X = OMe) [25], 14% (X = Ph) [26] and 66% (X = $CONH_2$) [27].

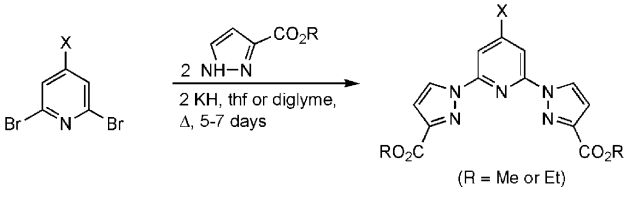

(2)

For this reason relatively few 2,6-di(pyrazol-1-yl)pyridines substituted at the pyridine ring have been made. Two groups, including the author's, have reported the synthesis of **35** [28] and **36**–**38** [29] in moderate-to-good yield from 2,6-dibromoisonicotinic acid [30]. Otherwise, the only 4-substituted-2,6-di(pyrazol-1-yl)pyridine derivatives that have been prepared in this way are those referred to in Eq. (2) (**9** and **39**–**41** [16,25–27], **42** [31,32] and **43** [27]).

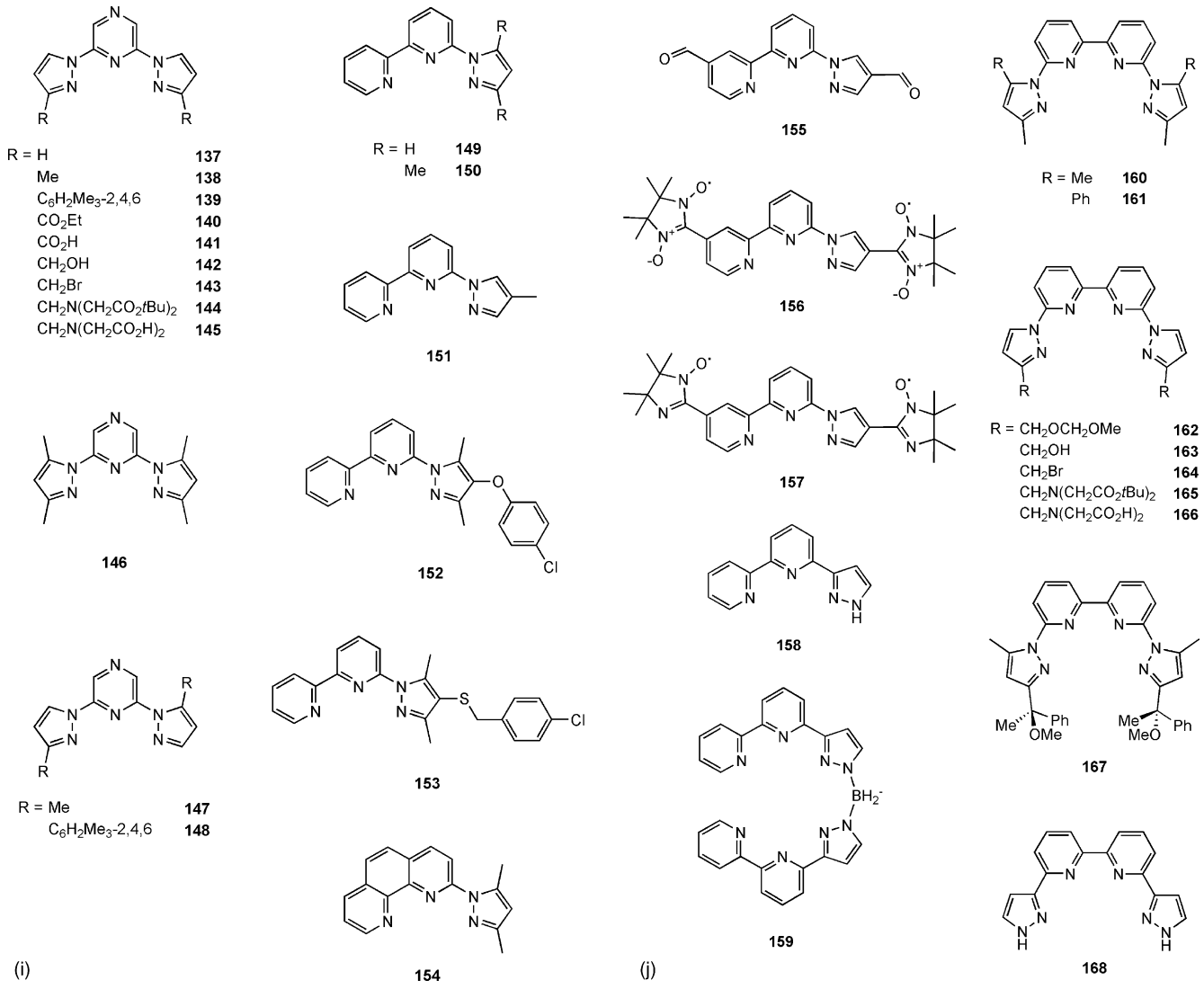

Scheme 1. (*Continued*).

In principle, a 2,6-di(pyrazol-1-yl)pyridine could also be prepared by treatment of 2,6-dihydrazinopyridine with 2 equiv. of a β-diketone or equivalent. Unfortunately, though, the poor availability of 2,6-dihydrazinopyridine [33] makes this impractical. Rather, the only other method that has been used to construct the 2,6-di(pyrazol-1-yl)pyridine framework is shown in Scheme 2, which yielded **44**–**46**; bromination of **46** subsequently gave **47** [34]. While several other 2,6-di(pyrazol-1-yl)pyridine ligands are also known, these have been made by functional group transformations subsequent to the initial pyridine/pyrazole coupling step. These are described below.

As can be seen from Eq. (1), the synthesis of substituted 2,6-di(pyrazol-1-yl)pyridines is simply a matter of obtaining the appropriately substituted pyrazole or dibromopyridine precursors before coupling them together. Several simple pyrazoles are commercially available, and many other 3{5}-alkyl or -aryl pyrazole derivatives can be prepared in good yields on a 10–100 g scale in two steps from an acyl precursor (Scheme 3) [35,36]. These are both reliable procedures, with the caveat that the hydrazine addition step sometimes has to be performed twice to go to completion [37]. Pyrazoles bearing other C-substitution patterns are also accessible through step (iii), although preparation of the appropriately substituted β-diketone (or equivalent) reagent is often more difficult [35]. Optically pure chiral pyrazoles for incorporation into 2,6-di(pyrazol-1-yl)pyridine have also been made in this way starting from appropriate terpenoid precursors [20–23]. An alternative, two-step procedure based on a [4 + 1] cyclisation step for 3{5}-alkyl or -aryl pyrazole synthesis has been more recently described (Scheme 4) [38]. This method can yield 4-substituted pyrazoles as well, although the yields are lower [39]. Once prepared, N–H pyrazoles can often be chlorinated or brominated at the C4-position [40],

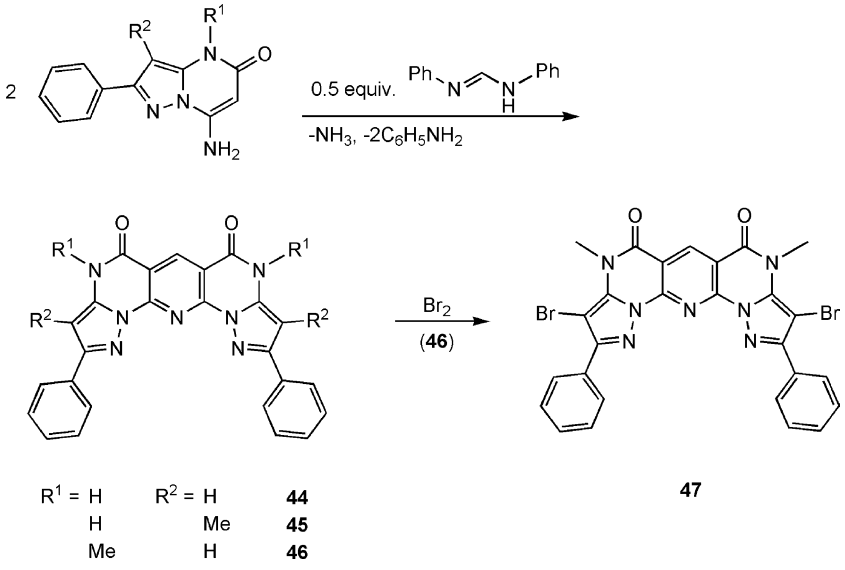

Scheme 2. Synthesis of annelated 2,6-di(pyrazolyl)pyridines by construction of the central pyridine ring [34].

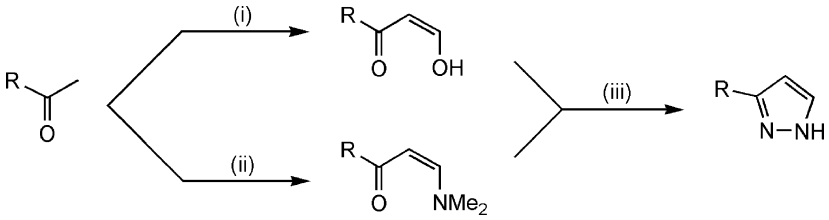

Scheme 3. Most commonly used synthetic routes to 3{5}-substituted pyrazoles from commercial starting materials, based on a [3 + 2] cyclisation of a β-diketone or equivalent with hydrazine. Reagents and conditions: (i) HCO_2Et, NaOMe, toluene, RT, 1–2 h. (ii) $Me_2NCH(OMe)_2$, reflux, N_2, 16 h. (iii) N_2H_4·HCl or N_2H_4·H_2O, MeOH, RT or reflux, 1–6 h.

but will add most other electrophiles to nitrogen rather than, or as well as, to carbon [41]. Lithiation of an N-protected pyrazole ring proceeds cleanly at C5, which has been used to prepare pyrazoles bearing 3{5}-benzyl, -arylsulfanyl and hydroxyalkyl functions by treatment with benzyl bromide, disulfide or ketone electrophiles, respectively [42]. A one-pot procedure for this type of transformation using formaldehyde protection of the pyrazole N–H group is given in [43]. Nonethe-less, it is generally more convenient to synthesise a NH pyrazole ring with the desired substitution pattern already in place.

While 2,6-dibromopyridine itself is commercially available and cheap, 4-substituted derivatives of this compound are harder to come by. Two routes into such compounds have proved useful for ligand synthesis. First, is that 2,6-dibromopyridine can be nitrated at the C4 position over three steps in 63% overall yield (Scheme 5) [44]. The nitro group in the resultant compound selectively undergoes nucleophilic substitution by NaOMe [25] or K[$SC_6H_4NO_2$-4] [44], yielding 4-methoxy- or 4-(4′-nitrophenylsulfanyl)-2,6-dibromopyridine in ca. 90% yield (Scheme 5). Alternatively, reduction of 2,6-dibromo-4-nitropyridine-N-oxide with iron powder yields 4-amino-2,6-dibromopyridine [45], whose amine group can be oxidatively substituted in ca. 50% yield by a phenyl [26] or thienyl [32] group (Scheme 5). 2,6-Dibromo-4-nitropyridine itself cannot be used to make a 2,6-dipyrazolylpyridine, since the pyrazolide nucleophile substitutes the nitro leaving group in preference to the bromide substituents [25]. Second, commercially available 2,6-dihydroxyisonicotinic acid can be doubly brominated by

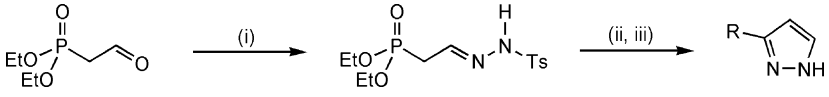

Scheme 4. Alternative synthetic route to 3{5}-substituted pyrazoles from commercial starting materials, based on a [4 + 1] cyclisation of a phosphorylacetaldehyde tosylhydrazone with an aldehyde (Ts = tosyl) [38,39]. Reagents and conditions: (i) TsN_2H_3, dil. HCl, 65 °C, 2 h. (ii) 2 equiv. NaH, thf, N_2, 0 °C-RT. (iii) RCHO, RT then reflux, 1–6 h.

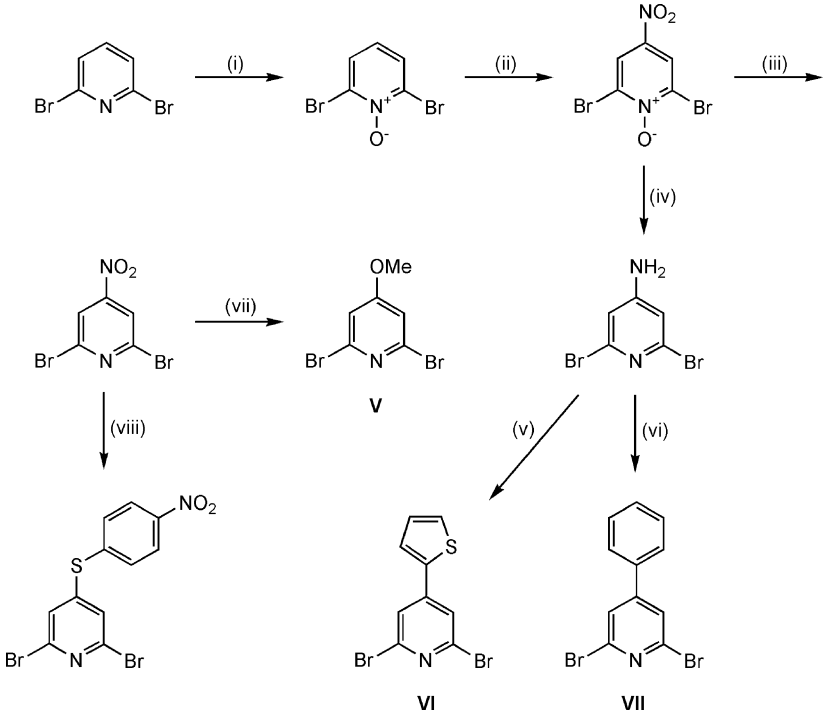

Scheme 5. Synthesis and transformations of 2,6-dibromo-4-nitropyridine [44,25–27,32]. Reagents and conditions: (i) aq. H_2O_2, CF_3CO_2H, 100 °C, 3 h. (ii) HNO_3/H_2SO_4, 100 °C, 1.5 h. (iii) PBr_3, CH_3CN, reflux, 14 h. (iv) Fe, CH_3CO_2H, 100 °C, 1 h. (v) C_4H_4S, CH_3CO_2H, isoamylnitrite, RT → 45 °C. (vi) C_6H_6, CF_3CO_2H, isoamylnitrite, RT → reflux. (vii) NaOMe, thf, 40 °C, 44 h. (viii) K[$SC_6H_4NO_2$-4], dmf, 60 °C, 3 h.

$POBr_3$ in 80% yield [30], and the resultant carboxylic acid derivative readily undergoes the usual functional group transformations [27,29,30] (Scheme 6). Compounds **V**–**IX** in Schemes 5 and 6 have been successfully used in Eq. (1) as precursors to 2,6-di(pyrazol-1-yl)pyridine derivatives, albeit in variable yields (see above).

A series of podands **15** and **48**–**52** have been prepared from pre-formed **9**, **39**–**43** following the reaction sequences shown in Scheme 7 [16,25–27,32]. Cumulative yields of these four-step syntheses are 20–30%. A similar sequence starting from **42**, with two added transformations at the thienyl function (shown in Scheme 7), also yielded the 5-aminothienyl-substituted derivative **53** [31]. Ester derivatives of most of these ligands (e.g. **16** [26]) have also been prepared, while a related sequence starting from **10** gave the amido derivatives **17** and **18** (yields for the latter compounds were not reported) [18]. Unsymmetric versions of **15** bearing a side-chain, **54**–**56**, have been prepared as their Tb(III) complexes through treatment of **12** with a mixture of two different iminodiacetate diester reagents (52% yield), followed by hydrolysis of the podand ester functions in the presence of $TbCl_3$ (60%) [46]. Succinimide-labelled **57** has also been reported, although no synthetic details were given [26,47]. Treatment of **13** (prepared from **12** in two steps via **14**) with diethylenetriamine penta(acetic acid) dianhydride yielded a mixture of the [1 + 1] and [2 + 2] macrocyclic products **58** and **59** in 10 and 20% yields, respectively [17]. The two compounds were separated by fractional crystallisation. The macrobicycle **60** was also synthesised in 30% yield, by reaction of **12** with 4,7,13,16-tetrabenzyl-1,4,7,10,13,16-tetraazacyclooctadeca-3,8,12,17-tetra-one in the presence of an alkali metal template [48]. Macrotricycle **61** was also a significant byproduct in this reaction. The macrobicycles **62** and **63** were prepared in a similar way, from diaza18crown6 and the appropriate 4-thienyl-2,6-bis(bromomethylpyrazolyl)pyridine reagent shown in Scheme 7 [31]. Esterification of **36** with half an equivalent of 1,3-propanediol yielded the binucleating ligand **64** [29].

The diradicals **65** and **66** were prepared in ca. 10% overall yield by reaction of **21** with 2 equiv. of 2,3-dimethyl-2,3-bis(hydroxylamino)butane at room temperature (**65**) or under reflux (**66**), followed by oxidation of the resultant hydroxylamines with periodate [19]. Toluene solutions of both compounds exhibit a half-field $\Delta m_s = \pm 2$ resonance by X-band EPR, which becomes more intense upon cooling to 4 K. This indicates that the nitroxyl radical centres in these compounds are ferromagnetically coupled to yield an S = 1 magnetic ground state. Fitting the temperature-dependence of the double integral of this signal yielded $2J = 11.8 \pm 4.8\ cm^{-1}$ between the radical centres for **65** [19]. An accurate value for $2J$ for **66** was not derived, but is clearly at least an order of magnitude smaller than for **65** (see also Section 6).

Finally, the propellenes **67** and **68** were synthesised in ca. 60% yield by reaction of pentafluoropyridine with 5 equiv.

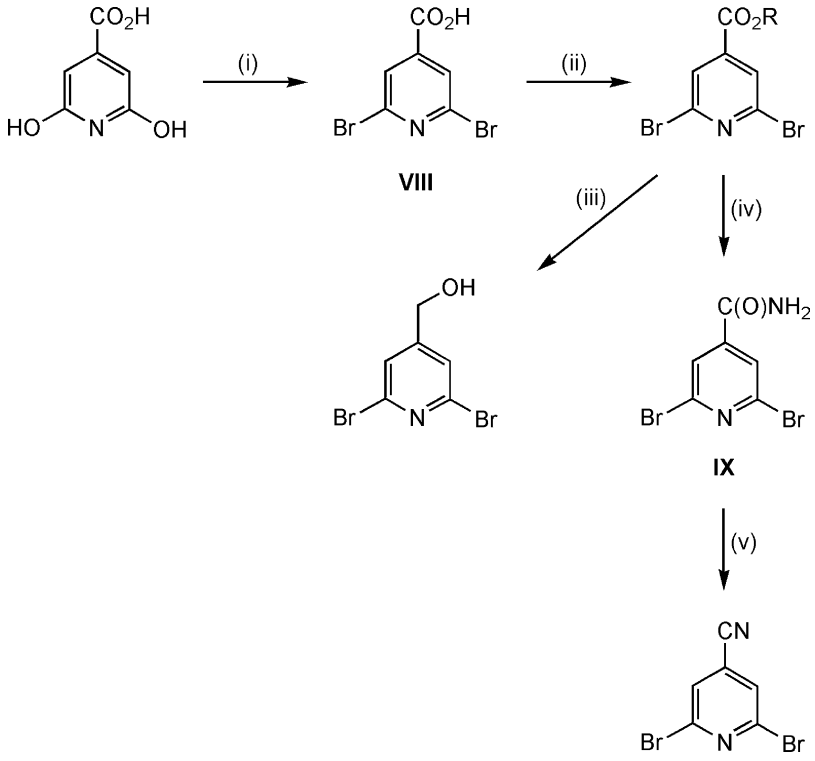

Scheme 6. Transformations of 2,6-dihydroxyisonicotinic acid [27,30]. Reagents and conditions: (i) $POBr_3$, 130 °C, 3 h. (ii) ROH (R = Me or Et), H_2SO_4 (cat.), reflux, 15 h. (iii) $NaBH_4$, EtOH, reflux, 15 h. (iv) NH_3, MeOH, 45 °C, 12 h. (v) P_2O_5, toluene, 100 °C, 48 h.

of the appropriate sodium pyrazolide salt [11]. Analogous reactions using fewer equivalents of pyrazolide yielded a mixture of low-yield products, including **67**, **68** and the tris- and tetrakis-pyrazolyl derivatives **71**–**74**. When a 1:1 ratio of pentafluoropyridine:pyrazolide was used, the 4-monopyrazolylpyridine species **X** was the highest yielding product (ca. 30%). Subsequent treatment of this intermediate with four more equivalents of a different pyrazolide reagent gave 80% yields of **69** and **70** [11].

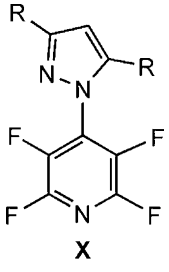

X

R = H or Me

Crystal structures of **1** [49], **4** [50], **5** [13], **19** [51] and **65** [19] have been reported, and all show the *transoid* dispositions of pyridine and pyrazole N-donors that is also found in terpyridines and related compounds [49]. The heterocyclic rings in these molecules are essentially coplanar, with dihedral angles between the least squares planes of the pyridine and pyrazole rings of 3.03(13)–7.8(2)°. The exception to this is **19**, which contains two unique molecules in its asymmetric unit [51]. While one molecule contains near-coplanar heterocyclic rings, as before, the other has one pyrazole moiety rotated by 40.4(1)° out of the plane of the pyridine ring. This difference is doubtless a consequence of the intermolecular steric environment surrounding this molecule in the crystal. All NMR studies of **1**–**64**, including sterically hindered examples like **27**, show a single conformation in solution that has the highest symmetry allowed by the chemical connectivity of the molecules. This implies that (presumably) except for the annelated examples **44**–**47**, the pyrazole and pyridine rings in these compounds can rotate freely with respect to each other on the NMR timescale (Fig. 1).

In the propellenes **67**–**69** the pyrazole groups are tilted from the planes of the pyridine rings by between 18.9(7) and 88.7(5)° (as measured from the C–C–N–N torsions linking the two heterocycles) [11]. This tilting is less severe for the 2- and 6-pyrazolyl substituents, which occupy less sterically crowded environments. Two different conformations were observed for these three compounds, depending the relative orientations of the pyrazole lone pairs above (*u*p) or below (*d*own) the pyridine ring. These are *ududd* (shown in Fig. 2) or *dudud*. NMR spectroscopy shows that the pyrazole rings of **67** and **69** have free rotation about their inter-heterocycle C–N bonds. However, the more sterically hindered **68** and **70** show two distinct isomeric structures in solution that do not interconvert on the NMR timescale, which were attributed

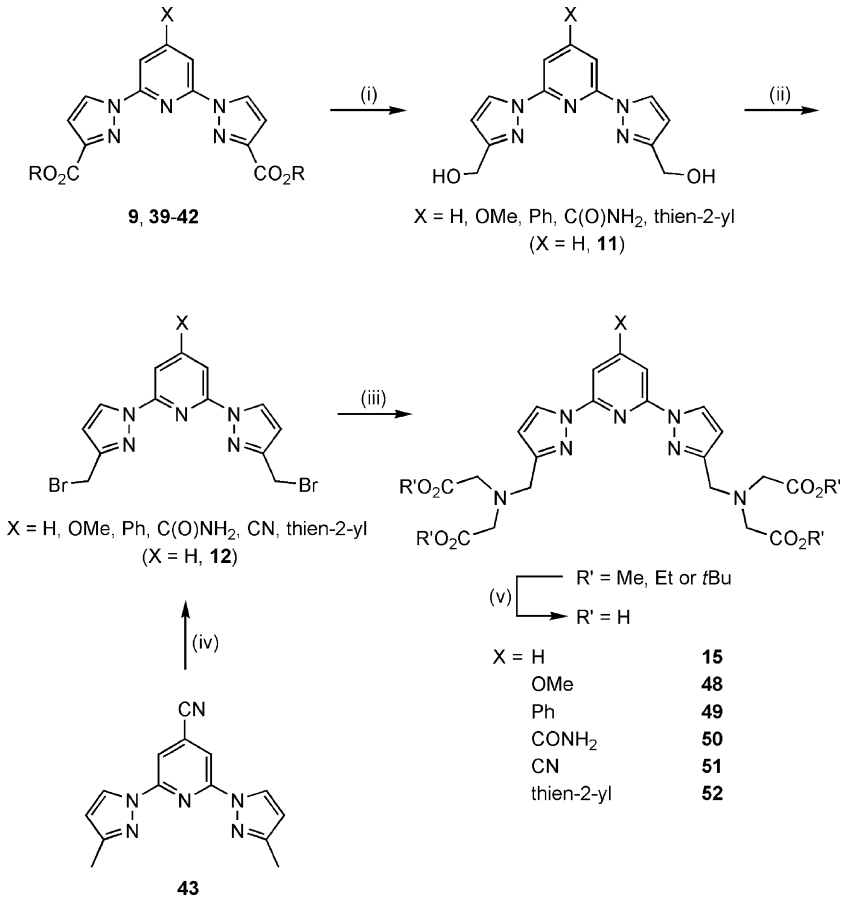

Scheme 7. Synthesis of podands containing a 2,6-di(pyrazol-1-yl)pyridine motif [16,25–27,32]. Reagents and conditions: (i) $LiAlH_4$, thf, 0 °C → RT, 1.5 h. (ii) PBr_3, CH_3CN, reflux, 1.5 h. (iii) $HN(C_2H_4CO_2R')_2$, Na_2CO_3, CH_3CN, RT, 24 h. (iv) *N*-Bromosuccinimide, CCl_4, $[PhC(O)O]_2$ (cat.), 80 °C, 2 h. (v) CF_3CO_2H, CH_2Cl_2, RT, 4 h.

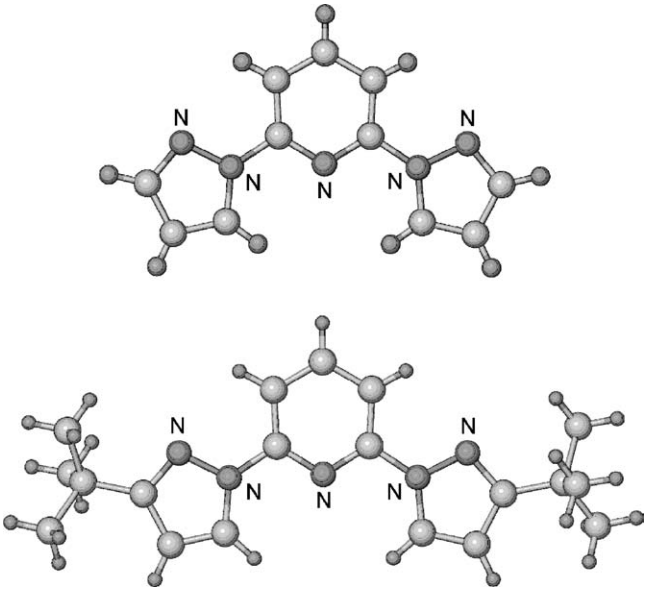

Fig. 1. Single crystal X-ray structures of **1** (top) [49] and **4** (bottom) [50], showing the *transoid*-antiperiplanar conformations of the pyridine and pyrazole rings.

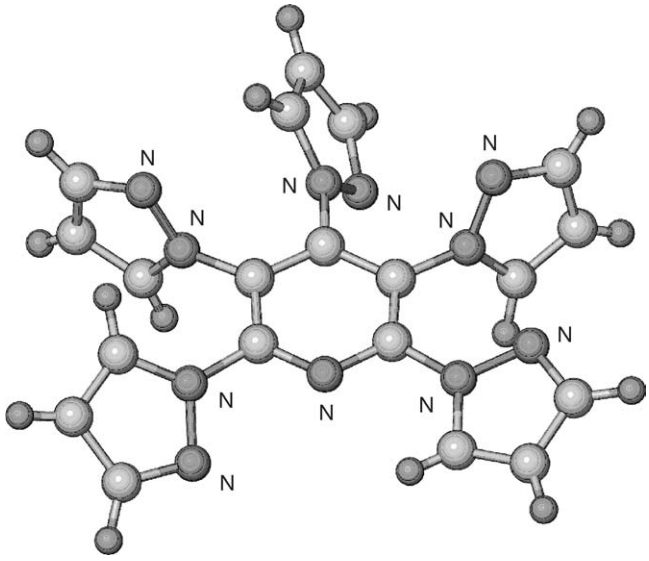

Fig. 2. Single crystal X-ray structure of **67** [11], showing the *ududd* disposition of the pyrazole lone pairs with respect to the pyridine ring.

to the two crystallographic conformations described above. Dipole moment measurements have implied that the ratio of *cisoid*:*transoid* conformations about each pyridine:pyrazole link at C2 and C6 of the pyridine rings is 15:85 for **67**, 55:45 for **71** and 30:70 for **73** [11]. No such measurements appear to have been carried out for any other of the ligands in this study, however.

2.2. Syntheses and structures of 2,6-di(pyrazol-3-yl)pyridines

The usual synthesis of the 2,6-di(pyrazol-3-yl)pyridine framework uses the methods shown in Scheme 2, starting from 2,6-diacetylpyridine. The parent ligand **75** is obtained in 75–95% overall yield according to Eq. (3) [36,52,53].

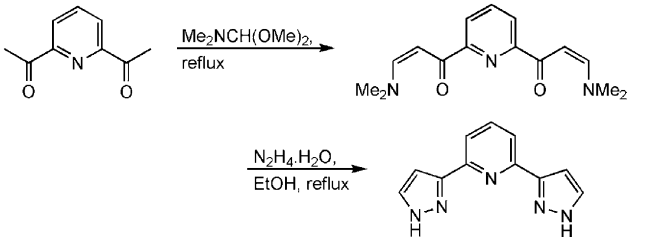

(3)

A small number of other derivatives of **75** functionalised at the pyrazole C atoms have also been made in a similar way, with the appropriate bis(1,3-diketonyl)pyridine intermediate being prepared via a Claisen condensation between the relevant ketone and pyridine-2,6-dicarboxylic acid, its diethylester or its dicarbonyl chloride [54–57]. A Stork reaction was also used in one case [56], although the same authors subsequently found the Claisen route to be more convenient [58]. Ligands **76** and **77** [54], **78** [55], **79** [56,58] and **80** [57] have been prepared in this way, with yields of 75–85%.

No 2,6-di(pyrazol-3-yl)pyridines derivatised at the pyridine ring have been made. However, functionalisation of the pyrazole NH groups in these ligands has been achieved in two ways (Scheme 8). Treatment of preformed **75** or **79** with an alkyl halide affords a mixture of two regioisomeric products **XI** and **XII**, with the bis-1,3-disubstituted regioisomer **XI** being the major species formed [52,58]. Formation of **XII** can be suppressed by coordination of **75** or **79** to Zn(II) [58] or Ru(II) [59], or by double deprotonation of the precursor ligand with BuLi, NaH or K_2CO_3 (which presumably leads to their chelation by the alkali metal) [57,58,60,65], before the alkylating agent is added. The following tridentate ligands have been prepared by this methodology: **81**, **84**, **86–89**, **91** and **92** [58], **82** and **83** (as their Ru(II) complexes only) [59], **85** [60], **90** and **94** [61], **93** [62], **95–97** [56], **98** [57], **99** and **100** [63], **101** [64] and **102** [65] (by alkylation of **75** and **76** with 2-bromopyridine), **103** [52] and **104** [66]. Reported yields of these disubstituted products range from 20 to 70%. Unsymmetrically substituted versions of **75** and **79** have also been obtained, using one or two sequential mono-deprotonation/alkylation sequences. This has yielded **106–112** [67], **113** [58], **114–116** and **119–122** [62], **117** [61] and **118** [68].

Alternatively, performing the second step of the synthesis of **75** or **79** (Eq. (3)) using 2 equiv. of an alkylhydrazine reagent instead gives the mixed isomer **XII** and the bis-1,5-disubstituted regioisomer **XIII**, in apparently variable product ratios [52,57,58]. The monoalkylated **XIV** was also observed as a byproduct in one case (Scheme 8) [52]. In one system, performing this step in the presence of a Zn(II) template changed the regiochemistry back in favour of isomer **XI** [58]. The diferrocenyl ligand **105** is the only new ligand of structure **XI** to have been made in this way, and was isolated in 31% yield [66]. The unfavourable regiochemistry of the hydrazine addition step of this synthesis was mitigated by synthesising the two pyrazole rings separately, and separating the 1,3- and 1,5-disubstituted pyrazole products after each step. The chemistry of ligands of type **XIII** has not been examined in depth, since they cannot chelate to a metal ion. Interestingly, however, there is one report of a related reaction of phenylhydrazine with 2,6-bis(3-napth-2-ylacryloyl)pyridine, yielding the potentially useful ligand **123** [69]. The origin of the different regiochemistries of these two types of reaction is unclear.

Two macrocycles containing the 2,6-di(pyrazol-3-yl)pyridine motif have been reported. **124** was synthesised in 18% yield by a Mannich reaction of **79** with 2-phenylethylamine and formaldehyde [56]. This product precipitated cleanly from the reaction mixture, so that no other products of the reaction were analysed. Treatment of **77** with di(chloromethyl)ether under phase transfer conditions yielded a mixture of the [2 + 2] cyclisation product **125**, and the [1 + 1] cyclisation product **127**, both in very low yields of 2–4% [54]. A similar reaction starting from **76** gave **126** only. The linear ditopic ligands **128** and **129** were synthesised almost quantitatively by alkylation of CH_2Cl_2 by 2 equiv. of deprotonated **113** or **114**, respectively [62]. One series of 2,6-bis(4,5-dihydropyrazol-3-yl)pyridine derivatives has also been made, namely **130–136**, by the same reaction sequence used to make **123** [69]. It was not explained why pyrazole (**123**) and dihydropyrazole (**130–136**) products are both obtained from otherwise identical reagents bearing different patterns of aryl substituent in this study.

Like all NH pyrazoles, **75–80** can exist as either their 3-pyridyl or 5-pyridyl tautomers (Eq. (4)) [70].

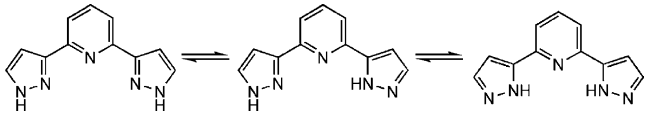

(4)

The single crystal X-ray structure of **75** shows both pyrazole rings to adopt the pyrazol-5-yl tautomer, with the N–H

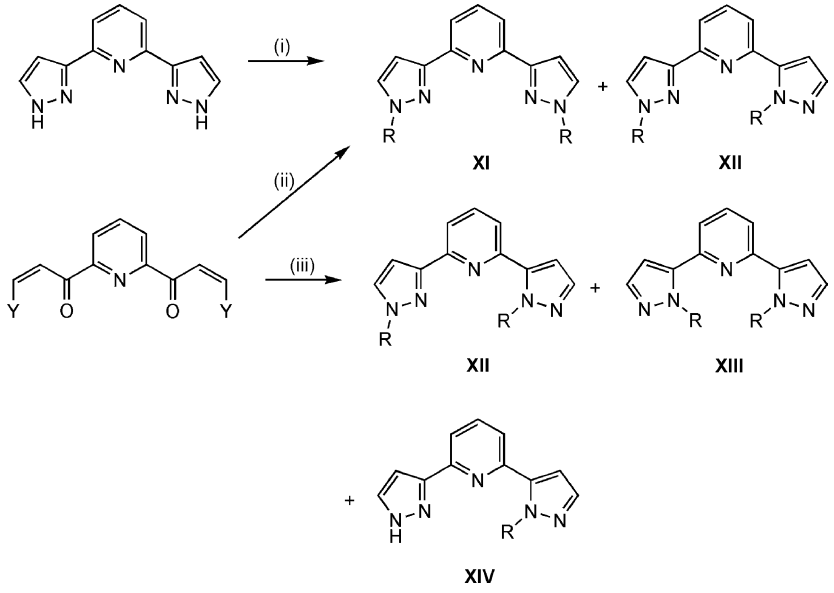

Scheme 8. Products of the synthesis of *N*-alkylated 2,6-di(pyrazol-3-yl)pyridines by different procedures (Y = OH or NMe_2). Reagents and conditions: (i) RBr or MeI, base. (ii) $RNHNH_2$, excess $ZnCl_2$, CH_2Cl_2, RT. (iii) $RNHNH_2$, $CHCl_3$, RT.

group adjacent to the pyridine ring [53,71]. In contrast to **1** and its derivatives (Section 2.1, Fig. 1), while the pyrazole and pyridine rings are near-coplanar (inter-ring dihedral angles 2.5 and 5.2°), the pyrazole N atoms in **75** are *cisoid* to the pyridine N donor (Fig. 3). The molecules in **75** are linked into 1D zig-zagged chains running parallel to the crystallographic *c* direction, through bifurcated intermolecular N–H···N···H–N hydrogen bonds (Fig. 3). The single crystal structure of **79** has an essentially identical molecular conformation to **75**, and contains two independent molecules in its asymmetric unit that are linked into dimers by a cyclic N-N-H…N-N-H double hydrogen bond [72] (this is a common motif in the intermolecular association of crystalline pyrazole derivatives [73]). In solution, the best technique for addressing the tautomeric states of pyrazoles is ^{13}C NMR [74]. Unfortunately, out of **75**–**80** ^{13}C spectra have only been reported for **78** and **79**. The pyrazole C3 and C5 ^{13}C resonances for **78** in $CDCl_3$ can be assigned at 154.01 and 145.3 ppm, respectively [55]. Using the criteria in ref. [74], these data are consistent with the 3-pyridyl tautomeric structure predominating in solution for this compound, in contrast to the two crystal structures discussed earlier in this paragraph. The same peaks are not present in the ^{13}C spectrum reported for **79** in $CDCl_3/CD_3OD$ [56], which implies that the tautomeric equilibrium in Eq. (4) is rapid on the NMR timescale [74].

In contrast to the above, the *N*-alkyl and *N*-aryl ligands **81** and **87** have *transoid* pyridine and pyrazole rings, that now resemble the 2,6-di(pyrazol-1-yl)pyridine structures (Fig. 4) [72]. However, steric repulsion between the annelated cyclo-

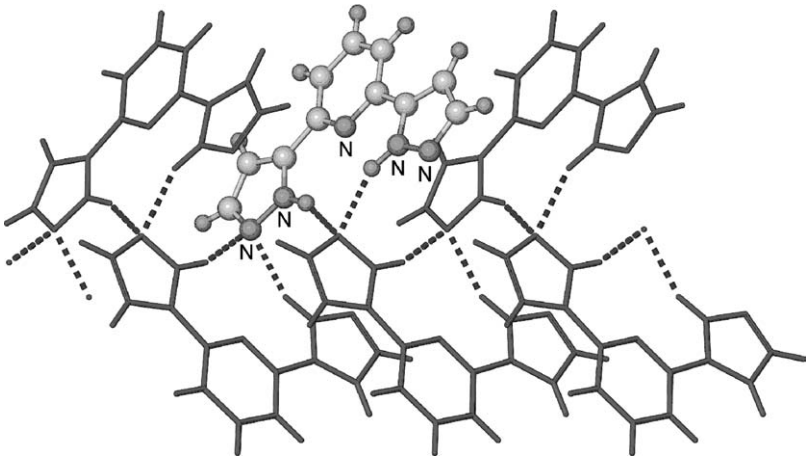

Fig. 3. Partial packing diagram of **75** in the single crystal [53,71], showing its association into zig-zag hydrogen-bounded chains.

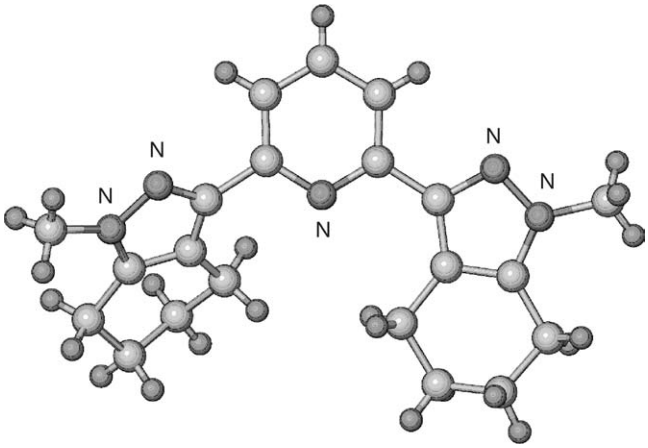

Fig. 4. Single crystal X-ray structure of **81** [72].

hexenyl groups in this conformation prevents their pyrazole rings from being coplanar with each other.

3. Metal complexes of 2,6-di(pyrazol-1-yl)pyridine ligands

3.1. Iron complexes

$[Fe(\mathbf{1})_2][BF_4]_2$ is high-spin at room temperature, but exhibits an abrupt and complete high → low-spin transition upon cooling to 261 K in the solid [75], or 248 K in acetone solution [76]. Anomalously, though, solid $[Fe(\mathbf{1})_2][PF_6]_2$ does *not* undergo spin-crossover, but remains fully high-spin between 5 and 300 K [76]. This behaviour is explained by the crystal structures of the two compounds: while $[Fe(\mathbf{1})_2][BF_4]_2$ has a six-coordinate geometry at iron with near-regular D_{2d} symmetry, the PF_6^- salt adopts an unusual C_2-distorted, twisted molecular structure that traps the complex in a high-spin state (Fig. 5). DF calculations showed that the C_2 structure represents a Jahn–Teller distortion of the high-spin d^6 manifold, and that it is favoured in complexes of tridentate ligands with narrow bite angles, like **1** [76]. Similarly distorted structures have also been seen in high-spin iron(II) complexes of two terpyridine derivatives [77]. The ClO_4^- and SbF_6^- salts of $[Fe(\mathbf{1})_2]^{2+}$ are isostructural with $[Fe(\mathbf{1})_2][PF_6]_2$, and also remain high-spin upon cooling [78]. The experimental molecular structures of high-spin and low-spin $[Fe(\mathbf{1})_2][BF_4]_2$ have been well-reproduced using combined QM/MM theoretical calculations [79]. The cyclic voltammogram of $[Fe(\mathbf{1})_2][PF_6]_2$ in acetone or MeCN solution shows an irreversible iron(II/III) oxidation near $E\mathrm{p}_a = +1.3$ V versus SCE [80].

Powdered $[Fe(\mathbf{1})_2][BF_4]_2$ also undergoes a light-induced excited spin-state trapping ('LIESST' [81]) transition upon laser irradiation at 5 K, to a metastable high-spin state that is stable for hours below 81 K [82]. Irradiation of a single crystal of this material also yields a trapped high-spin excited state, without crystal degradation, which is long-lived

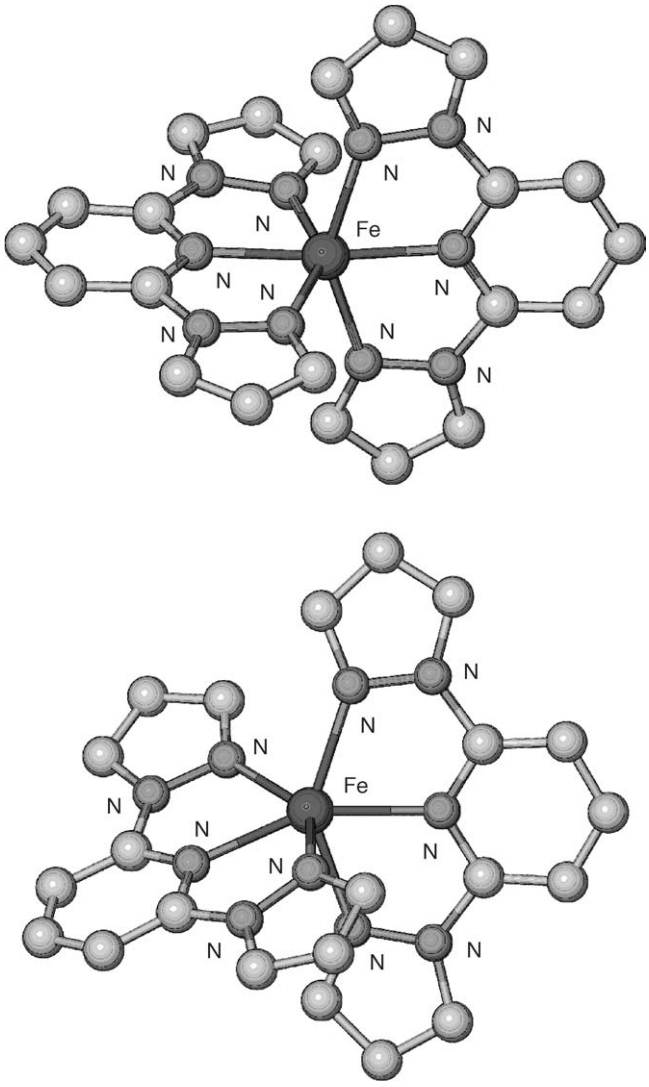

Fig. 5. Views of the complex dications in the single crystal structures of $[Fe(\mathbf{1})_2][BF_4]_2$ (top) and $[Fe(\mathbf{1})_2][PF_6]_2$ (bottom), showing the angular Jahn–Teller distortion exhibited by the latter compound [76]. For clarity, all H atoms have been omitted. The complex dications in other $[M(\mathbf{1})_2][BF_4]_2$ crystal structures (M = Co [12], Ni [12], Cu [15,93–95] and Zn [94]) are visually indistinguishable from the top figure, with Fe replaced by the appropriate metal.

enough to be crystallographically characterised [83]. The same crystallographic experiment has also been performed using $[Fe(\mathbf{35})_2][BF_4]_2$, which has very similar spin-crossover and LIESST characteristics to $[Fe(\mathbf{1})_2][BF_4]_2$ [28]. Interestingly, for both compounds the molecular structures of the thermally populated high-spin state at room temperature, and of the photochemically trapped high-spin state at 30 K, are almost identical to within experimental error. This contrasts with most of the published crystallographic studies of this type on other compounds, where the iron centres in the two different high-spin structures show significant structural differences [84]. This has been explained by anisotropic crystal contraction upon cooling, which means that the anisotropic crystal pressure experienced by molecules in crystals of these

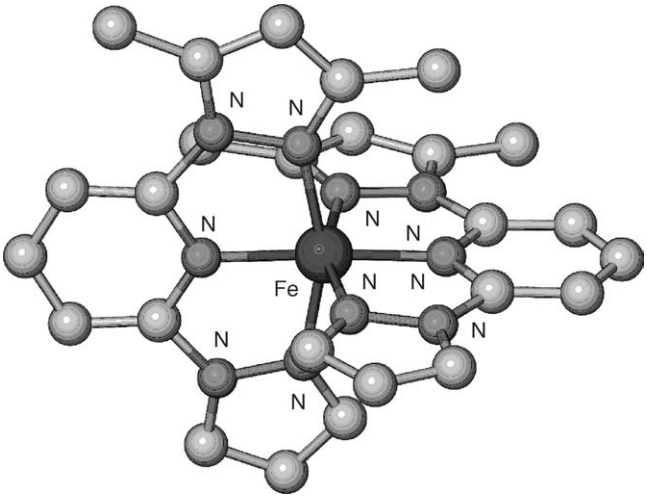

Fig. 6. View of the complex dication in the single crystal structure of $[Fe(\mathbf{32})_2][BF_4]_2$ [88]. For clarity, all H atoms have been omitted. Fe–N bond lengths 1.8939(16)–1.9714(18) Å.

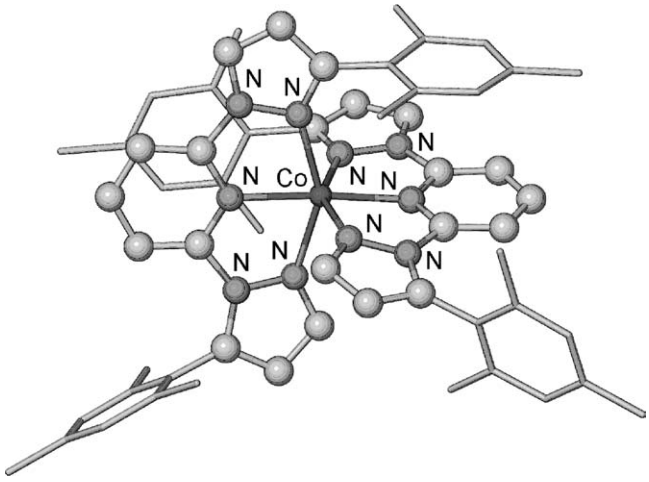

Fig. 7. View of the complex dication in the single crystal structure of $[Co(\mathbf{27})_2][BF_4]_2{\cdot}4MeCN$ [12]. For clarity, all H atoms have been omitted and the ligand mesityl substituents have been de-emphasised.

compounds is very different at 293 K and 30 K. The reason why $[Fe(\mathbf{1})_2][BF_4]_2$ and $[Fe(\mathbf{35})_2][BF_4]_2$ behave differently is uncertain, but it may be related to the 'terpyridine embrace' crystal packing motif [85] that is exhibited by both compounds.

The salts $[Fe(\mathbf{3})_2]X_2$ ($X^- = BF_4^-$ and PF_6^-), $[Fe(\mathbf{6})_2][BF_4]_2$ and $[Fe(\mathbf{9})_2][BF_4]_2$ are all fully high-spin between 5 and 300 K in the solid, and between 180 and 300 K in acetone solution [78,86]. In contrast, however, $[Fe(\mathbf{8})_2]X_2$ ($X^- = BF_4^-$, PF_6^- [86] and $1/2[FeCl_4]^{2-}$ [87]) are both fully low-spin over the same temperature range. Consideration of the spin-states of these compounds led to the following ranking of donor strengths of four of these ligands: $\{\mathbf{3},\mathbf{6}\} < \mathbf{1} < \mathbf{8}$. The positioning of **3** as a weak field ligand in this series is anomalous, since the electron-donating *iso*propyl groups should increase the basicity of its pyrazole donors. This anomaly was attributed to inter-ligand steric repulsion in these complexes involving the *iso*propyl substituents, which could lengthen the M–N{pyrazole} bonds on steric grounds [78,86]. Solid $[Fe(\mathbf{32})_2][BF_4]_2$ is low-spin at room temperature (Fig. 6) [88], but undergoes a spin-state transition in CD_3NO_2 solution centred at 288 ± 2 K. The five-coordinate complexes $[FeX_2(\mathbf{19})]$ ($X^- = Cl^-$ and I^-) have been prepared; the crystallographically characterised chloride complex adopts a distorted square-pyramidal geometry, with the basal and apical Fe–Cl bond lengths being almost equal [51]. $[FeCl_2(\mathbf{8})]$ undergoes rapid ligand disproportionation in MeCN to yield $[Fe(\mathbf{8})_2][FeCl_4]$ [87].

The salt $[Fe(\mathbf{11})_2][ClO_4]_2$ crystallises as mixtures of two or three crystal forms from common organic solvents [89]. Two of these are solvent-free polymorphs, which are both high-spin at 100 K. That may reflect the fact that the iron centres in both crystals exhibit a less severe form of the same angular Jahn–Teller distortion found in $[Fe(\mathbf{1})_2][PF_6]_2$ (see above; Fig. 5). A solvate, of formula $[Fe(\mathbf{11})_2][ClO_4]_2{\cdot}x$MeCN ($x \approx 0.75$), is fully high-spin at 200 K but undergoes a partial spin-state transition upon cooling to 100 K, as evidenced by a yellow-to-brown colour change and by the appearance of conformational disorder in one of the two ligands [89]. Refinement of this disorder implied that the transition was 42% complete at this temperature. Interestingly the packing diagram of the compound at 100 K reveals that the hydroxyl group of the low-spin ligand disorder site is only 1.456(17) Å from its nearest neighbour when that molecule is also low-spin. This strongly implies that only one complex molecule in this pair can be low-spin at any time, to avoid this steric clash, and places a natural limitation of 50% completeness on the spin-state transition. This represents a new mechanism by which an incomplete spin-crossover can occur in a solid containing a single unique iron site. In contrast to this complicated behaviour, $[Fe(\mathbf{11})_2][BF_4]_2$ crystallises as a single high-spin phase [78].

3.2. Other first row transition metal complexes

Two series of compounds $[CoL_2][BF_4]_2$ and $[NiL_2][BF_4]_2$ (L = **1**, **3**, **6** and **8**) have been synthesised [12]. All the cobalt compounds are high-spin at room temperature. Single crystal structures for the **1** and **8** complexes of both metal ions show the expected distorted octahedral geometries, with the mesityl substituents in the latter compounds having minimal steric influence on the M–N (M = Co and Ni) bond lengths. The d–d absorption maxima shown by both series of complexes imply that the ligand field exerted by the four ligands follows the trend $\mathbf{3} \approx \mathbf{6} < \mathbf{1} < \mathbf{8}$. This is the same trend derived for the corresponding iron(II) complexes in the previous paragraph. $[Co(\mathbf{1})_2][PF_6]_2$ exhibits a quasi-reversible cobalt(II/III) couple by voltammetry in acetone, at $E_{1/2} \approx +1.0$ V versus SCE which is ca. 0.65 V more positive than that of $[Co(terpy)_2]^{2+}$ [80]. The complexes $[Co(\mathbf{8})_2][NO_3]_2$ [90] and $[Co(\mathbf{27})_2][BF_4]_2{\cdot}4MeCN$ (Fig. 7) [12] have also been crystallographically characterised, the

latter being the only reported complex of a ligand of structure **III** to date (Section 2.1). The five-coordinate compounds $[CoX_2(\mathbf{19})]$ ($X^- = Cl^-$, N_3^-, NCS^-) have been synthesised and show irreversible cobalt-based voltammetric oxidations [91]. The crystal structure of the thiocyanate compound shows a cobalt coordination geometry midway between that of a square pyramid and trigonal bipyramid. The complex $[Ni_2(N_3)(\mu\text{-}N_3)_2(\mathbf{19})_2]$ contains end-on bridging azido ligands by crystallography, and exhibits irreversible voltammetric oxidations and reductions [92].

Homoleptic $[Cu(\mathbf{1})_2][BF_4]_2$ exhibits a $\{d_{x^2-y^2}\}^1$ ground state by EPR spectroscopy, which corresponds structurally to a pseudo-Jahn–Teller elongation along one of its two N{pyrazole}–Cu–N{pyrazole} axes [15,93–95]. The Cu–N bond lengths in this compound are temperature-dependent, reflecting dynamic disorder of the Jahn–Teller elongation axis over the two different N{pyrazole}–Cu–N{pyrazole} vectors in the molecule. The energetics of this fluxionality have been analysed in some detail [94,95]. Unusually, crystals of $[Cu(\mathbf{1})_2][BF_4]_2$ undergo a phase change at 41 K, involving a tripling of the unit cell *b* dimension in the low temperature phase but no change in the space group of $P2_1$ [93]. This allows every third molecule in the crystal to rotate its axis of pseudo-Jahn–Teller elongation by 90° with respect to the others, yielding the antiferrodistortative distribution of Jahn–Teller elongations within the crystal that is commonly preferred in such compounds [96]. In contrast to these results, $[Cu(\mathbf{6})_2][BF_4]_2$ [97] and $[Cu(\mathbf{8})_2]X_2$ ($X^- = BF_4^-$ or ClO_4^-) [15,24] exhibit a rhombically compressed structure, leading to a $\{d_{z^2}\}^1$ electronic ground state [98]. This is caused by steric repulsion between the mesityl groups of one ligand and the pyridine ring of the other, which are sandwiched together on one side of the complex periphery. These were the first molecular copper(II) compounds to have this property [97], although it has since been reproduced in other, related compounds [99,100]. Strictly speaking, this structure does not correspond to a Jahn–Teller compression, because the copper $3d_{x^2-y^2}$ and $3d_{z^2}$ orbitals are not degenerate in the ideal D_{2d} symmetry of these molecules in the absence of the distortion. Rather, it is a very rare example of a quenched (pseudo)-Jahn–Teller distortion [97]. Interestingly the asymmetrically substituted complex $[Cu(\mathbf{31})_2][ClO_4]_2$, bearing one mesityl group per ligand, exhibits a normal pseudo-Jahn–Teller elongated structure identical to that shown by $[Cu(\mathbf{1})_2][BF_4]_2$ [24]. That shows that four mesityl groups-worth of steric repulsion per molecule are required to enforce the change in ground state at the copper centre.

Although $[Cu(\mathbf{6})_2]^{2+}$ and $[Cu(\mathbf{8})_2]^{2+}$ are stable compounds, the *tert*butyl substituents in **4** are too large to allow $[Cu(\mathbf{4})_2]^{2+}$ to form. Rather, reactions of L^4 with copper(II) salts yielded $[CuCl_2(\mathbf{4})]$, $[Cu_2(\mu\text{-}Cl)_2(\mathbf{4})_2][BF_4]_2\cdot nH_2O$ ($n = 0$ or 2) and $[Cu(solv)_2(\mathbf{4})][BF_4]_2$ (solv = H_2O or MeCN) [101]. The two dimeric compounds, and $[Cu(NCMe)_2(\mathbf{4})][BF_4]_2$, all show rather distorted [4 + 1 + 1] six-coordinate copper(II) centres by crystallography. Interestingly, solid $[Cu(NCMe)_2(\mathbf{4})][BF_4]_2$ converts to $[Cu(OH_2)_2(\mathbf{4})][BF_4]_2$ within minutes upon exposure to atmospheric moisture. All of these copper(II)/**4** complexes are strongly solvatochromic, which for $[CuCl_2(\mathbf{4})]$ reflects partial decoordination of **4**, rather than the Cl^- ligands, from the copper centres in solution [101]. The copper ions in $[CuBr_2(\mathbf{1})]$ and $[Cu_2(\mu\text{-}Br)_2(\mathbf{1})_2][ClO_4]_2$ [102] show coordination geometries similar to those of the **4**-containing complexes, implying that the structural distortions shown by the latter are not a consequence of steric crowding. Crystallisation of a mixture of $Cu[NO_2]_2$ and **19** from H_2O:MeCN yields crystals with the unusually complicated formula $\{[\{Cu(NO_2)(\mathbf{19})\}_2(\mu\text{-}NO_2\text{-}\kappa N{:}\kappa O)]^+[Cu(NO_2)_2(\mathbf{19})]\}_2[Cu(NO_2)_4]^{2-}\cdot$MeCN [103]. Both the neutral and cationic copper species in this structure have a [4 + 1 + 1] six-coordinate stereochemistry, with asymmetrically bidentate terminal nitrite ligands. Single crystal structures of $[CuCl(N_3)(\mathbf{19})]$ [104] and $[Cu(NCMe)(isonicotinamide)(\mathbf{1})][BF_4]_2\cdot$2MeCN [105] have also been reported, both of which have slightly distorted square pyramidal copper centres with apical Cl^- and MeCN ligands, respectively.

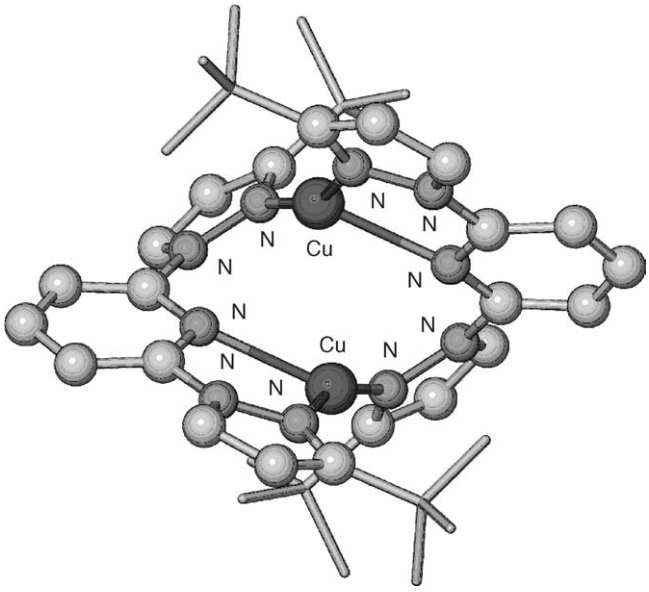

Fig. 8. View of the complex dication in the single crystal structure of $[Cu_2(\mu\text{-}\mathbf{4})_2][PF_6]_2$ [106]. For clarity, all H atoms have been omitted and the ligand *tert*butyl substituents have been de-emphasised.

As with related meridional tris-imine ligands [4], **1**, **4** and **8** form helical dimer complexes with copper(I) [106]. Interestingly the single crystal structures of $[Cu_2(\mu\text{-}\mathbf{1})_2][PF_6]_2$, $[Cu_2(\mu\text{-}\mathbf{4})_2][PF_6]_2$ and $[Cu_2(\mu\text{-}\mathbf{8})_2][BF_4]_2\cdot 2(CH_3)_2CO$ all show different metal ion stereochemistries, with different combinations of two, three- and four-coordinate copper centres in each compound. In particular, $[Cu_2(\mu\text{-}\mathbf{4})_2][PF_6]_2$ is unusual for complexes of this type, in being formed from three-coordinate copper(I) centres (Fig. 8). Although the two ligand *tert*butyl environments in $[Cu_2(\mu\text{-}\mathbf{4})_2][PF_6]_2$ are equivalent by ^{1}H NMR at room temperature, their resonances decoalesce in $(CD_3)_2CO$ at 198 K, implying that the helical

structure may be maintained in this solvent. That being the case, a free energy of activation of 43.5 kJ mol^{-1} was derived for migration of the copper ion between pyridine donors [106]. However, voltammetric measurements implied that the principle copper(I) species present in MeCN solutions of $[Cu_2(\mu\text{-}\mathbf{4})_2][PF_6]_2$ is in fact $[Cu(NCMe)_4]^+$ [101]. Addition of 2.5 equiv. of **23**–**25** to copper(I) triflate yields catalysts for the cyclopropanation of styrene by ethyl diazoacetate [22]. Although yields were good (49–82%), only moderate *cis*:*trans* selectivity (1:2) and e.e.s (12–66%) were obtained. It is uncertain what the active catalysts are in these mixtures since no copper(I) species were isolated in this work, although it was postulated that tetrahedral $[CuL_2]^+$ (L = **23**–**25**) complexes with bidentate 'L' ligands might be involved [22].

Crystal structures of $[Zn(\mathbf{1})_2][BF_4]_2$ [94] and $[Zn(\mathbf{8})_2][ClO_4]_2{\cdot}2MeNO_2$ [107] have been described, and show the expected near-regular six-coordinate structures.

3.3. Ruthenium complexes

The complexes $[RuL_2]^{2+}$ (L = **1**, **19** and **32**), and the mixed-ligand $[Ru(\mathbf{1})L']^{2+}$ (L′ = **19** and **32**) and $[Ru(\mathbf{19})(\mathbf{32})]^{2+}$, have been synthesised [108]. The reversible Ru(III/II) redox couples in this series of compounds showed an almost perfectly linear dependence on the number of methyl substituents at the ligand periphery, decreasing from +1.25 V versus SCE for $[Ru(\mathbf{1})_2]^{2+}$ to +1.06 V for $[Ru(\mathbf{19})_2]^{2+}$. The UV–vis spectrum of $[Ru(\mathbf{1})_2]^{2+}$ shows a lowest lying MLCT absorption at 377 nm (26,525 cm^{-1}), 5500 cm^{-1} higher in energy than for $[Ru(terpy)_2]^{2+}$. In addition, $[Ru(\mathbf{1})_2]^{2+}$ undergoes a ligand-based reduction at a potential 0.41 V more negative than $[Ru(terpy)_2]^{2+}$. These absorption and redox data imply that **1** is both a weaker π-acceptor, and a weaker σ-donor, than terpy and has a substantially higher π^* orbital energy [108]. For these reasons it was predicted that $[Ru(\mathbf{1})_2]^{2+}$ should not be luminescent [109], although that does not seem to have been verified experimentally. Only one mixed-ligand ruthenium(II) terpy/2,6-di(pyrazol-1-yl)pyridine complex has been made, $[Ru(ttpy)(\mathbf{19})][PF_6]_2$, which is inert to photochemical ligand substitution by MeCN [110].

Trans-$[RuCl_2(PMe_3)L]$ (L = **1**, **6**, **7** and **19**) have been synthesised by addition of 1 equiv. of PMe_3 to $[RuCl_3L]$ in the presence of excess NEt_3 [14]. Photolysis of *trans*-$[RuCl_2(PMe_3)(\mathbf{1})]$ and *trans*-$[RuCl_2(PMe_3)(\mathbf{6})]$ with a tungsten lamp converts them to their *cis*-isomers in good yield. Treatment of $[RuCl_3L]$ (L = **1**, **6**, **7** and **19**) with 2 equiv. of PMe_3 in the presence of zinc amalgam, followed by tungsten lamp photolysis in the presence of $NaClO_4$, yields *trans*-$[RuCl(PMe_3)_2L]ClO_4$ [14,111]. The latter were converted to *trans*-$[RuNO_2(PMe_3)_2L]ClO_4$ with $NaNO_2$, and then to *trans*-$[RuNO(PMe_3)_2L]ClO_4$ by treatment with $HClO_4$ [14]. $[RuCl(PMe_3)_2(\mathbf{6})]ClO_4$ [111], and all four nitro compounds [14], were crystallographically characterised. The Ru–N{pyrazole} bond lengths in the latter

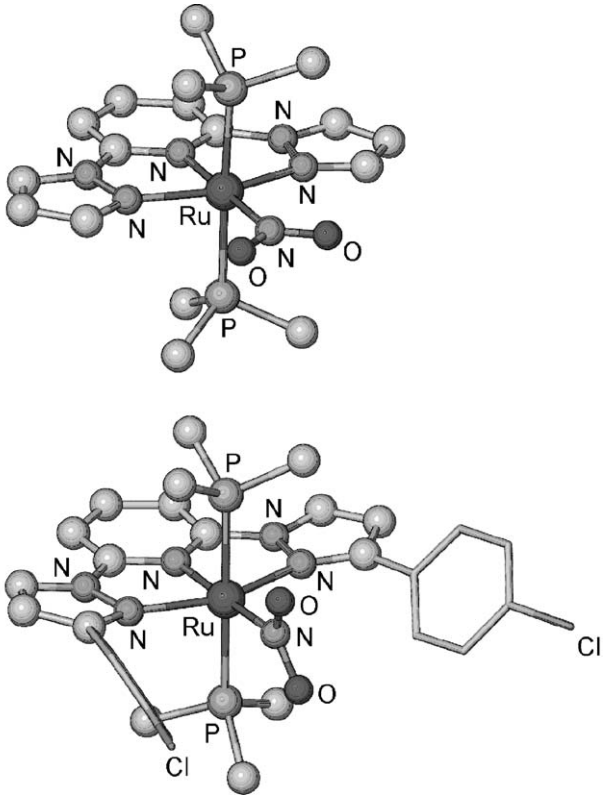

Fig. 9. Views of the complex cations in the single crystal structures of $[RuNO_2(PMe_3)_2(\mathbf{1})]ClO_4$ (top) and $[RuNO_2(PMe_3)_2(\mathbf{7})]ClO_4$ (bottom), showing the different orientations of the nitro ligands in the two compounds [14]. For clarity, all H atoms have been omitted, and the ligand 4-chlorophenyl substituents in the bottom figure, have been de-emphasised.

series were significantly longer for the compounds containing phenyl ligand substituents (i.e. **6** and **7**). Interestingly, the nitro ligand in $[RuNO_2(PMe_3)_2(\mathbf{1})]ClO_4$ lies in the plane of the **1** ligand, while in the other three compounds it is close to perpendicular to it (Fig. 9). Both these structural effects were attributed to the intramolecular steric influences of the different dipyrazolylpyridine ligands used. Comparison of the crystal structure of the **1** complex with that of $[RuNO_2(PMe_3)_2(terpy)]ClO_4$ [112], led to the suggestion that **1** is sterically smaller than terpy. The *trans*- and *cis*-$[RuCl_2(PMe_3)L]$, $[RuCl(PMe_3)_2L]ClO_4$ and $[RuNO(PMe_3)_2L]ClO_4$ compounds listed above all show a chemically reversible Ru(III/II) couple by voltammetry [14,111]. However, while the Ru-based oxidation of $[RuNO_2(PMe_3)_2(\mathbf{1})]ClO_4$ is also reversible, $[Ru^{III}NO_2(PMe_3)_2L]^{2+}$ (**6**, **7** and **19**) all decompose at the anode to yield $[Ru^{II}NO(PMe_3)_2L]^+$ through an ECE mechanism [14]. The rate of decomposition appeared to correlate with the steric bulk of the L ligand in these compounds, leading to the suggestion that the instability of $[Ru^{III}NO_2(PMe_3)_2L]^{2+}$ was sterically induced [14].

Treatment of $[RuCl_2(PPh_3)_3]$ with 1 equiv. of **1** yields a mixture of *cis*- and *trans*-$[RuCl(PPh_3)_2(\mathbf{1})]Cl$, in an approximately 80:20 ratio, while interestingly a similar reac-

tion using **19** affords *trans*-[$RuCl_2(PPh_3)$(**19**)] only [113]. Reaction of [{$RuCl_2$(cymene)}$_2$] with **19** in the presence of C_2H_4 yields *trans*-[$RuCl_2(\eta^2$-$C_2H_4)$(**19**)], while *trans*-[$RuCl_2$(CO)(**19**)] and *trans*-[$RuCl_2$(NCMe)(**19**)] were synthesised by treatment of [$RuCl_3$(**19**)] with the appropriate monodentate ligand in refluxing MeOH in the presence of excess Et_3N. Treatment of *trans*-[$RuCl_2(\eta^2$-$C_2H_4)$(**19**)] with phenylethyne gives *cis*-[$RuCl_2$(=C=CHPh)(**19**)], while reaction of *trans*-[$RuCl_2(PPh_3)$(**19**)] with HC≡CC(OH)Ph_2 and $AgBF_4$ affords [RuCl(=C=C=CPh_2)(PPh_3)(**19**)]BF_4, in which the phosphane ligand is *trans* to the **19** pyridyl donor [113]. A series of β-diketonate complexes has also been made, [RuCl(RC{O}CHC{O}R′)L] (L = **1**, **19** and **32**; R = R′ = Me {acac}, Ph, *t*Bu or CF_3; R = Me, R′ = CF_3: **XV**), from the appropriate [$RuCl_3$L] and β-diketone precursors in refluxing EtOH and Et_3N as before [114]. The chloride ligands in [RuCl(acac)(**1**)] and [RuCl(acac)(**19**)] were readily substituted by the nitrogenous bases imidazole, 4,4′-bipyridine, pyrazine and/or MeCN, to yield six-coordinate cationic products. The Ru(III/II) half-potentials in these compounds showed a linear relationship with the Hammett σ_M constants of the β-diketonate R and R′ substituents [114].

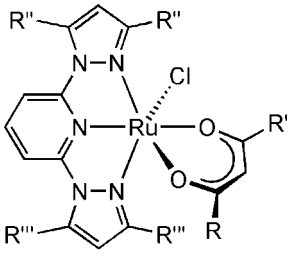

XV

R = R' = Me, Ph, *t*Bu, CF_3 or R = Me, R' = CF_3
R'' = R''' = H, Me or R'' = H, R''' = Me

Treatment of [$RuCl_3$(**19**)] with bipy, phen or Me_2bipy in refluxing EtOH and Et_3N yields [RuCl(diimine)(**19**)]PF_6 [115]. These were converted to [Ru(solv)(diimine)(**19**)][PF_6]$_2$ (solv = H_2O or MeCN) by treatment with $AgPF_6$ in the appropriate solvent. The [RuCl(diimine)(**19**)]PF_6 complexes all show a reversible Ru(III/II) oxidation by voltammetry. However oxidation of [Ru(OH_2)(diimine)(**19**)][PF_6]$_2$ is pH-dependent in the range $2 \leq pH \leq 11$, implying that oxidation to ruthenium(III) is accompanied by deprotonation of the aqua ligand [115]. No second oxidation to a ruthenium(IV) oxo species was detected, in contrast to the corresponding [Ru(OH_2)(diimine)(terpy)]$^{2+}$ system [116]. However, [Ru(OH_2)(bipy)(**22**)]$^{2+}$ (Fig. 10) does show both Ru(III/II) and Ru(IV/III) couples by voltammetry (E° = +0.83 and +0.98 V versus SCE at pH 1.1), and is oxidised cleanly by mCPBA to isolable [RuO(bipy)(**22**)]$^{2+}$ [117]. A variety of styrene derivatives were epoxidised stoichiometrically by [RuO(bipy)(**22**)][ClO_4]$_2$, in yields of 22–70% and with e.e.s of 30–38%; the corresponding benzaldehydes were often significant byproducts in these reactions [117]. These

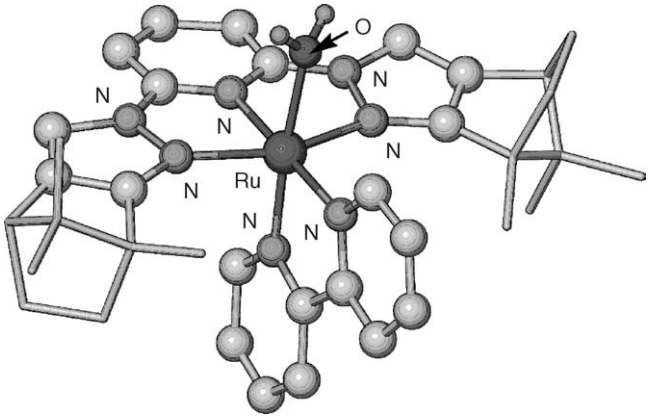

Fig. 10. View of the complex dication in the single crystal structure of [Ru(OH_2)(bipy)(**22**)][ClO_4]$_2$·2H_2O [117]. For clarity, all C-bound H atoms have been omitted.

reactions proceed by a stepwise free-radical mechanism, and the moderate e.e.s obtained in this system may be partly due to rapid *cis*/*trans* isomerisation of the benzylic radical intermediate [118].

The complexes [RuX(dcbipy)(**19**)]PF_6 (X = Cl^- [119] or NCS^- [120]) both show an unassigned visible absorption at λ_{max} = 569–587 nm ($\varepsilon_{max} \approx 5000\ M^{-1}\ cm^{-1}$), which is not exhibited by the chloro/dimine complexes described earlier, in addition to the usual MLCT peaks at lower wavelength. Prototype TiO_2 solar cells containing both compounds as sensitisers showed quite promising photo-energy conversion efficiencies of up to 1.7%, with the NCS^- complex being a more efficient photosensitiser than the Cl^- one [121]. A resonance Raman spectroelectrochemical investigation has revealed the presence of I_3^-, produced from the iodide-containing electrolyte, which associates closely with the [RuX(dcbipy)(**19**)]$^+$ molecules at the TiO_2 surface in these solar cells [122].

3.4. Other second and third row transition metal complexes

Reaction of [$ReX(CO)_5$] (X = Cl^-, Br^- or I^-) with one of three 2,6-di(pyrazol-1-yl)pyridines yields the octahedral compounds *fac*-[$ReX(CO)_3$L] (L = **1**, **19** and **32**) containing bidentate 'L' ligands by NMR [123]. These compounds are fluxional in solution through chemical exchange between the metal-bound and free pyrazole donors, which occurs by a concerted 'tick-tock' mechanism via a seven-coordinate transition state. The free energies of activation for this fluxional processes, derived from variable temperature NMR, follow the trend in L of **1** (least basic) < **32** < **19** (most basic). One similar reaction under more forcing conditions yielded instead *cis*-[$ReBr(CO)_2$(**32**)], in which **32** is now tridentate by NMR [123].

Treatment of [$RhCl_3$L] (L = **24** and **25**) with 2 equiv. of AgTf in thf yields moderately active catalysts for the cyclopropanation of styrene by ethyl diazoacetate [22]. While

there was no *cis*:*trans* selectivity in the product mixtures, the catalysts containing **24** and **25** gave encouraging (and opposite) e.e.s of 80–85%. Interestingly, the favoured product enantiomers isolated from these reactions were the opposite to those isolated from analogous reactions catalysed by copper(I) complexes of the same ligands (Section 3.1) [22]. The reason for these differences is uncertain.

Addition of **1** to [PdClMe(cod)] did not yield a well-defined product. However, the same reaction performed with the addition of AgTs yielded [PdMe(**1**)]Ts [124]. Surprisingly, ^{1}H NMR at 223 K in CD_3OD shows this compound to contain bidentate **1**. Presumably the fourth coordination site at the palladium centre is occupied by coordinated tosylate or solvent, although this was not pursued further. As for the rhenium complexes described earlier, at room temperature the palladium ion undergoes rapid chemical exchange between the coordinated and free pyrazole rings. Since the corresponding compound [PdMe(terpy)]Cl contains a tridentate terpy ligand, the bidentate coordination of L^1 in [PdMe(**1**)]Ts was ascribed to the poorer basicity of the pyrazole donors in **1**. Consistent with this, **1** is completely solvolysed from the palladium ion when this compound is dissolved in dmso. Unusually, [PdMe(**1**)]Ts does not react with CO, unlike the terpy complex which rapidly yields $[Pd(C\{O\}Me)(terpy)]^+$ [124]. The cause of this differing reactivity is unclear.

The complexes $[PtClL]Cl{\cdot}H_2O$ and $[PtPhL]PF_6$ (L = **1** and **19**) have been prepared, by treatment of the appropriate tridentate ligand with K_2PtCl_4, or with [PtClPh(cod)] and $AgPF_6$, respectively [109]. Single crystal structures of $[PtCl(\mathbf{1})]Cl{\cdot}H_2O$ and $[PtPh(\mathbf{1})]PF_6{\cdot}MeCN$ show the expected square-planar complex cations, arranged through intermolecular π–π interactions into linear stacks (Fig. 11). Interestingly, while the other three complexes in this series are only weakly emissive, $[PtPh(\mathbf{1})]PF_6$ exhibits a strong, narrow emission spectrum centred at 655 nm under UV irradiation at 77 K. Glassy solutions of this compound do not fluoresce in this way. Although the solid state emission resembles that shown by several solid $[PtCl(terpy)]^+$ compounds, the platinum centres in adjacent molecules in the crystal of $[PtPh(\mathbf{1})]PF_6{\cdot}MeCN$ are too far apart (4.5–4.7 Å) to allow $5d_{z^2-z^2}$ overlap between them (which is the usual origin of emissions in these solids [6]; Fig. 11). Hence, the origin of the fluorescence in solid $[PtPh(\mathbf{1})]PF_6$ is not known.

The single crystal structures of $[Cd_2(NCO)_2(\mu\text{-}NCO)_2(\mathbf{19})_2]$ and $[Cd_2(NCS)_2(\mu\text{-}NCS)_2(\mathbf{19})_2]$ have been reported [125]. While the cyanato complex contains 'end-on' μ-1,1-NCO^- ligands, the bridging ligands in the thiocyanato complex have a 'end-to-end' μ-1,3-NCS^- coordination mode.

3.5. Lanthanide complexes

Europium(III) and terbium(III) complexes of the tetracarboxylate podands **15** [16,126], **48** [25,126], **49** [25], **50** [26], **51** [27] and **52** [32] (Scheme 6) have been generated in situ by mixing aqueous solutions of a simple salt of the relevant metal and the appropriate ligand. Aqueous solutions of samarium(III) and dysprosium(III) complexes of all these ligands except **49** and **52** have also been prepared in a similar manner [27,127], as have gadolinium(III) complexes of **15** and **48** [126]. No solid complexes have been isolated from these mixtures, nor have any structural characterisation data been presented. However, luminescence decay time measurements of the all the europium and/or terbium complexes yielded hydration numbers (q) of $0.3–0.5 \pm 0.5$ [16,25–27,32]. That is, the lanthanide ions contain no aquo ligands to within experimental error, and are perfectly encapsulated by the (potentially nonadentate) podands. All of these lanthanide/podand solutions luminesce upon UV irradiation of a ligand $n \rightarrow \pi^*$ transition [128], with the terbium (τ = 2.28–2.82 ms and ϕ = 0.51–1.00 at room temperature) and europium (1.28–1.38 ms and 0.02–0.16) complexes

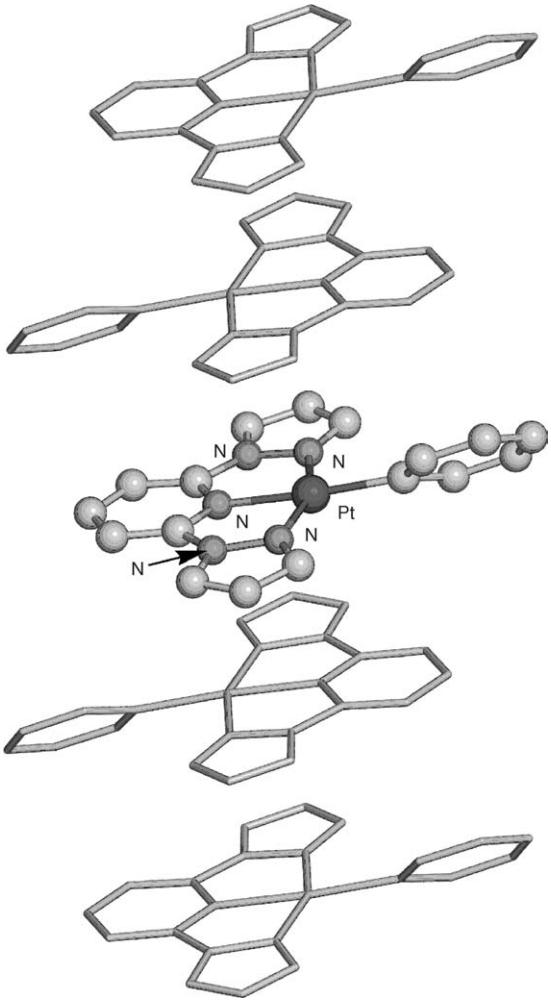

Fig. 11. Partial packing diagram of $[PtPh(\mathbf{1})]PF_6{\cdot}MeCN$, showing the arrangement of the complex cations into stacks [109]. The Pt centres in adjacent molecules in these stacks are separated by 4.5–4.7 Å. For clarity, all H atoms have been omitted.

having particularly useful emissions [16,25–27,32,46,126]. The terbium compounds of **49** [26] and **50** [27] are of particular interest, in that they show almost perfectly efficient ligand → metal energy transfer which results in emission quantum yields (ϕ) approaching unity. The energies of the ligand triplet excited states for **15**, **48**, **50** and **51**, measured from their Gd complexes, follow an apparent Hammett relationship from their pyridine substituents with $\rho = -8.7$ [27]. Since energy transfer from this triplet state is the origin of metal-based luminescence in these compounds [128], that explains why pyridine substitution has such an effect on the emissiveness of the lanthanide complexes of this ligand series. A similar correlation has also been reported from a much larger study of europium and terbium complexes of 41 different chelates, including **15** and **48** [126].

The terbium(III) complexes of **54**–**56**, when bound through their side-chains to a model protein, showed luminescence yields (i.e. $\phi{\cdot}\varepsilon$) that were only 30–40% lower than for the Tb/**15** parent complex [46]. Similarly, binding of **49** to the polypeptide streptavidin (via its succinimide monoester **57**) gave a conjugate whose terbium(III) complex showed a reduced, but still useful, emission quantum yield of 0.58 [26]. The latter conjugate complex was used in a time-resolved fluoroassay, to sense the proteins α-fetoprotein and carcinoembryonic antigen in human serum at the pg cm^{-3} level [26,47]. The streptavidin-labelled [Tb(**49**)] species has been grafted onto the 3′-end of a stretch of DNA, that also bears an organic dye at its 5′ terminus. Irradiation of the terbium centre causes strong emission from the organic dye when the DNA strand is hybridised to a probe DNA sequence [129]. The terbium/**49** complex has also been doped into silica nanoparticles of 42–45 nm diameter [130,131], which have then been coated with streptavidin [130] and α-fetoprotein antigen [131] as before. These bioconjugated fluorescent nanoparticles can respectively sense human prostate-specific antigen at the 70 pg cm^{-3} level [130], and α-fetoprotein to 100 pg cm^{-3} [131]. The uses of luminescent lanthanide complexes of **53** [31] and **54**–**56** [132] for biological sensing applications have been patented. The macrocycles **58** and **59**, respectively form 1:1 and 1:2 adducts with aqueous terbium(III), having $q = 1.1 \pm 0.5$ molecules per metal [17]. Adducts between trivalent lanthanide ions and the cryptands **60** and **61** both have a 1:1 stoichiometry by mass spectrometry [48]. The europium and terbium complexes of **58**–**61** all show similar luminescence lifetimes and quantum yields to the podand ligands in the previous paragraph.

Europium and gadolinium complexes of diamide ligand **17** have been used as reagents in sol gel syntheses [18]. The europium-containing gels are luminescent, with an excited state half-life of 0.64 ms. This is ca. 50% shorter than the solid europium complex of **18**, which was also prepared as a reference. The absorption spectra of the gels at 15 K showed the presence of two distinct europium sites, which may differ in their degree of hydration.

4. Metal complexes of 2,6-di(pyrazol-3-yl)pyridine ligands

4.1. Main group metal complexes

Ligands **81** and **86** solubilise sodium picrate into chloroform, while their regioisomers of type **XII** (Scheme 8) do not [58]. Similarly, **128** reacts with excess sodium picrate in $CDCl_3$ to sequentially afford adducts with the formula [Na(**128**)$_2$]pic and [{Na(μ-**128**)}$_2$]pic$_2$ by NMR [62]. The pentadentate ligands **95**–**97** form 1:1 complexes with alkali metal picrates in $CHCl_3$, with log K of 3.8–5.2, although the selectivity of these ligands for different metals was small [56]. The macrocycle **125** extracts a variety of group 1 and group 2 metal picrates, and ammonium picrate, from neutral aqueous solution into CH_2Cl_2 with ca. 60% efficiency [54]. None of the picrate complexes in this paragraph were isolated from solution.

4.2. Iron complexes

Different salts of $[Fe(\mathbf{75})_2]^{2+}$ have proven to show a wide variety of thermal and photochemical high → low-spin-state transitions, several of which have been studied in detail (Table 1). While the temperatures of these transitions vary greatly, it can be generalised that hydration of the compounds tends to favour the low-spin form of the complex. Hence, hydrates of the Br^-, I^- [133,145], NO_3^- [133], BF_4^-, ClO_4^- [134], PF_6^- [145], Tf^- [138] and $[Cr(C_2O_4)_3]^-/ClO_4^-$ [143] salts of $[Fe(\mathbf{75})_2]^{2+}$ are all low-spin at room temperature. However, all of these apart from the NO_3^- salt can be dehydrated upon heating to anhydrous phases that are high-spin at room temperature and undergo spin-crossover upon cooling. In acetone solution, spin-crossover in different salts of $[Fe(\mathbf{75})_2]^{2+}$ takes place with $T_{1/2} \approx 260$–270 K [133]. DF calculations suggested that $[Fe(\mathbf{75})_2]^{2+}$ should be low spin at 0 K in the gas phase, contrary to what is observed in condensed phases [144].

Three of the solids in Table 1 have been studied in particular detail. Anhydrous $[Fe(\mathbf{75})_2][BF_4]_2$ undergoes an abrupt high → low-spin transition centred at 176 K, with a hysteresis loop of between 10 and 16 K depending on the measurement [134–137,145]. Rapid freezing of the sample to 77 K results in trapping of the (now metastable) high-spin state, which only relaxes back to its low-spin form upon rewarming to above ca. 90 K [135,136]. The metastable high-spin state of $[Fe(\mathbf{75})_2][BF_4]_2$ can also be photogenerated (the 'LIESST' effect [81]), and is stable below ca. 80 K. The rate of thermal relaxation of the metastable high-spin state in this compound generated by freeze-quenching or irradiation is similar but, unusually, does not follow first-order kinetics [136]. That spin-crossover is accompanied by a crystallographic phase change in both $[Fe(\mathbf{75})_2][BF_4]_2$ and $[Fe(\mathbf{75})_2]Tf_2{\cdot}H_2O$ (see below) was confirmed by EPR measurements of Mn^{2+} centres doped into these materials [146].

Table 1
Summary of spin-state transitions undergone by different anhydrous and hydrated salts of $[Fe(\mathbf{75})_2]^{2+}$

	$T_{1/2}$ (K)	ΔT (K)	Character	Reference
$[Fe(\mathbf{75})_2]Br_2$	252	4	Abrupt	[133,145]
$[Fe(\mathbf{75})_2]Br_2{\cdot}5H_2O$[a]	340	0	Gradual	[133,145]
$[Fe(\mathbf{75})_2]I_2$	203	2	Abrupt	[133]
$[Fe(\mathbf{75})_2]I_2{\cdot}2H_2O$	256	0	Abrupt	[145]
$[Fe(\mathbf{75})_2]I_2{\cdot}4H_2O$[a]	330	0	Gradual	[133,145]
$[Fe(\mathbf{75})_2][NCS]_2{\cdot}2H_2O$	227	0	Gradual, discontinuous	[140,141,145]
$[Fe(\mathbf{75})_2][NCSe]_2$	231	2	Abrupt	[140,141]
$[Fe(\mathbf{75})_2][NO_3]_2{\cdot}2H_2O$	≈243	0	Gradual	[133]
$[Fe(\mathbf{75})_2][BF_4]_2$	176	10	Abrupt	[134–136,145]
$[Fe(\mathbf{75})_2][BF_4]_2{\cdot}2H_2O$[a]	>300	0	Gradual	[133]
$[Fe(\mathbf{75})_2][BF_4]_2{\cdot}3H_2O$	288	0	Gradual	[133,145]
$[Fe(\mathbf{75})_2][ClO_4]_2$	220	0	Gradual	[134]
$[Fe(\mathbf{75})_2][ClO_4]_2{\cdot}H_2O$	280	0	Gradual	[134]
$[Fe(\mathbf{75})_2][ClO_4]_2{\cdot}3H_2O$[a]	330	0	Gradual	[134]
$[Fe(\mathbf{75})_2][PF_6]_2$	171	2	Abrupt, 50% complete	[133,145]
$[Fe(\mathbf{75})_2][PF_6]_2{\cdot}H_2O$	≈177	0	Gradual, discontinuous	[133]
$[Fe(\mathbf{75})_2][PF_6]_2{\cdot}2H_2O$	≈243	0	Gradual, discontinuous	[133]
$[Fe(\mathbf{75})_2][PF_6]_2{\cdot}3H_2O$[a]	355	0	Gradual	[145]
$[Fe(\mathbf{75})_2]Tf_2$	≈230	N/a	Gradual, ≈50% complete	[138]
$[Fe(\mathbf{75})_2]Tf_2{\cdot}H_2O$	140↓ 170, 285↑	≈140	Abrupt, discontinuous in warming mode	[138,139]
$[Fe(\mathbf{75})_2]Tf_2{\cdot}3H_2O$[a]	355	N/a	Gradual	[138]
$[Fe(\mathbf{75})_2][Fe(CN)_5(NO)]$	182	3	Abrupt	[142]
$[Fe(\mathbf{75})_2]_2[Cr(C_2O_4)_3]ClO_4{\cdot}5H_2O$[a]	≈375	≈20	Gradual	[143]

[a] Transition is accompanied by water loss from the sample.

In contrast, $[Fe(\mathbf{75})_2]Tf_2{\cdot}H_2O$ exhibits in cooling mode an abrupt and complete high → low-spin transition at 140 K. However, upon rewarming the low → high-spin conversion takes place in two steps: a gradual transition centred at 170 K during which ca. 1/3 of the sample becomes high-spin; and, a more abrupt change at 285 K [139]. This leads to the bulk of the sample showing a very wide spin-crossover hysteresis width of ca. 140 K. A metastable high-spin form of $[Fe(\mathbf{75})_2]Tf_2{\cdot}H_2O$ can also be generated at 77 K by freeze-quenching or irradiation [139]. Unlike the BF_4^- compound, though, the relaxation kinetics of this metastable state at higher temperatures depend strongly on the method used to generate it. To explain this it was suggested that freeze-quenching the sample preserved the high-temperature crystallographic phase, while LIESST excitation generated a metastable high-spin form of the low-temperature phase [139].

Finally, fresh samples of $[Fe(\mathbf{75})_2][NCS]_2{\cdot}2H_2O$ undergo a gradual spin-transition upon cooling, which is split into two steps centred at 205 and 252 K [140,141]. Unusually for a gradual spin-state transition, both of these steps exhibit hysteresis loops, which are respectively 26 and 9 K in width. Repeated cycling of this transition changes the behaviour of the sample, so that it shows a single, more abrupt spin-crossover at 232 K; annealing of the sample at room temperature for 24 h led to its reversion to the original two-step spin-crossover [141]. This unusual behaviour was attributed to reversible disruption of the intermolecular hydrogen bond network in the material during repeated thermal cycling.

The LIESST relaxation temperatures of eight different anhydrous or hydrated salts of $[Fe(\mathbf{75})_2]^{2+}$ have been measured and compared [145]. An approximate linear relationship was found in these compounds, between the thermal spin-crossover $T_{1/2}$ and the LIESST relaxation temperature. The origin of this correlation is uncertain, although similar effects have also been observed for other series of chemically related iron(II) compounds [147].

Despite this complex behaviour, relatively few of the compounds in Table 1 have been crystallographically characterised. Of those that have, $[Fe(\mathbf{75})_2]I_2{\cdot}4H_2O$, $[Fe(\mathbf{75})_2][BF_2]_2{\cdot}3H_2O$ [133], $[Fe(\mathbf{75})_2]Tf_2{\cdot}3H_2O$ [138] and $[Fe(\mathbf{75})_2]_2[Cr(C_2O_4)_3]ClO_4{\cdot}5H_2O$ [143] are low-spin at room temperature, while $[Fe(\mathbf{75})_2][NCS]_2{\cdot}\ 2H_2O$ and $[Fe(\mathbf{75})_2][NCSe]_2$ are high-spin and $[Fe(\mathbf{75})_2][NCSe]_2{\cdot}H_2O{\cdot}CH_3NO_2$ is in a mixture of spin-states [140]. The only compound in this series for which a variable temperature crystallography study has been achieved is $[Fe(\mathbf{75})_2][Fe(CN)_5(NO)]$ [142]. This compound undergoes a crystallographic phase change, from *P*4/*ncc* (high-spin) at room temperature to a *Pnca*:*Pncb* twin (low-spin) at 100 K. This transition is accompanied by a significant reorganisation of the nitroprusside anions in the lattice, and explains the strongly cooperative spin-crossover exhibited by this compound. Interestingly the low-spin crystal structure of $[Fe(\mathbf{75})_2][BF_2]_2{\cdot}3H_2O$ [133] is inconsistent with its spin-crossover $T_{1/2}$ of 288 K measured from a powder sample, which implies the compound should be mostly high-spin at room temperature [145]. The reason for this discrepancy is unclear.

4.3. Other first row transition metal complexes

Crystals of $[M(\mathbf{75})_2][Cr(C_2O_4)_3]ClO_4{\cdot}6H_2O$ (M = Co and Ni) are isostructural with the corresponding iron(II) pentahydrate salt, and have been crystallographically characterised [143]. These compounds show no detectable magnetic interactions between the complex dications and $[Cr(C_2O_4)_3]^{3-}$ anions. The salt $[Cu(\mathbf{75})_2]BF_4[SiF_6]_{0.5}$ was crystallised from a mixture of L^{71} and $Cu[BF_4]_2$, the Si content of the crystals originating from the glass crystallisation vessel [148]. The copper centre in this compound exhibits a crystallographically ordered pseudo-Jahn–Teller-elongated structure (cf. $[Cu(\mathbf{1})_2][BF_4]_2$, Section 3.2). Ligand **78** extracts nickel(II) and cobalt(II), but not iron(II), into kerosene from sulfuric acid leaches in the presence of dinonylnaphthalenesulfonic acid ([DNNSA]H), as the complex $[M(\mathbf{78})_2][DNNSA]X$ (M = Co or Ni, X^- = an unknown anion) [55].

The compounds $[CoCl_2(\mathbf{75})]$ [149] and $[CuX_2(\mathbf{75})]$ (X^- = Cl^- and Br^-) [148] all exhibit mononuclear structures by crystallography, with coordination geometries that are mid-way between those of a square-pyramid and a trigonal bipyramid ($\tau \approx 0.5$ [150]). The 1:1 $Co[ClO_4]_2$ complex of **79**, generated in situ, catalyses the aqueous hydrolysis of 4-nitrophenyl acetate, albeit with small rate enhancements of 2–5.7 over the uncatalysed reaction [60]. The 1:1 iron(II), nickel(II) and copper(II) complexes of **79**, and the cobalt(II) complexes of **85** and **89**, are catalytically inactive under the same conditions. The $ZnTf_2$ complex of **98**, also prepared in situ, catalyses the asymmetric Diels Alder reaction of 1-acryloyl-3,5-dimethylpyrazole with cyclopentadiene with e.e.s of up to 75% [57]. Addition of $ZnBr_2$ to a $CDCl_3$ solution of **128** yielded an adduct with a C_2-symmetric ^1H NMR spectrum, that was tentatively formulated as $[\{ZnBr_2\}_2(\mu\text{-}\mathbf{128})]$ [62].

Potentially pentadentate **101** forms a tetranuclear complex with copper(II) acetate $[\{Cu_2(\mu\text{-}O_2CMe)_2(\mu\text{-}\mathbf{101})(\mu_3\text{-}OH)\}_2][PF_6]_2{\cdot}2MeOH$. This is comprised of two $[Cu_2(\mu\text{-}O_2CMe)(\mu\text{-}\mathbf{101})(\mu\text{-}OH)]^+$ fragments held within a bis-bidentate **101** ligand, that are linked by additional weak axial Cu···OH interactions (Fig. 12) [64]. The compound behaves as a Curie-Weiss paramagnet above 100 K, with $\theta = 2$ K. The mononuclear compound $[CoCl_2(\mathbf{101})]$ has also been crystallised, in which **101** acts as a tridentate ligand with both terminal pyridyl groups non-coordinating [149]. Reaction of the related ligand **102** with $[Cu(NCMe)_4]PF_6$ affords a double helical trinuclear complex $[Cu_3(\mu_3\text{-}\mathbf{102})_2(NCMe)_2][PF_6]_3$, in which all three copper(I) centres are tetrahedral [65].

4.4. Ruthenium complexes

The complexes $[Ru(\mathbf{79})_2]Cl_2$ [56] and $[Ru(\mathbf{81})_2]Cl_2$ [72], and $[RuL_2][PF_6]_2$ (L = **79**, **81**–**83**, **87**, **88**, **90**, **91**, **93**, **94**, **113**, **114** and **117**) [61], have been synthesised. The heteroleptic compounds $[Ru(\mathbf{81})(L')][PF_6]_2$ (L′ = **87** and **113**) were also obtained, via the intermediate complex $[RuCl_3(\mathbf{81})]$

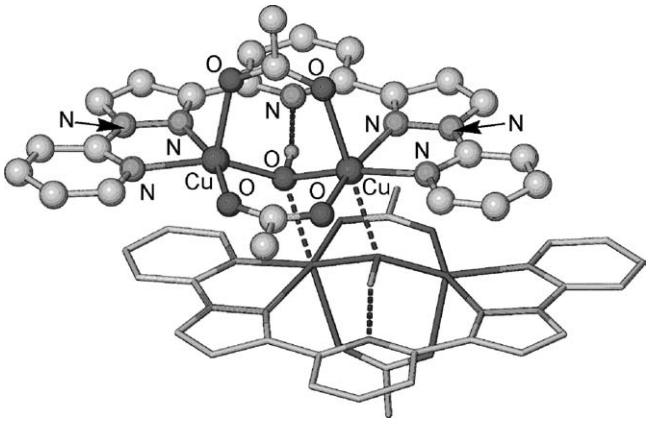

Fig. 12. View of the complex dication in the single crystal structure of $[\{Cu_2(\mu\text{-}O_2CMe)_2(\mu\text{-}\mathbf{101})(\mu_3\text{-}OH)\}_2][PF_6]_2{\cdot}2MeOH$ [64]. For clarity, all C-bound H atoms have been omitted and one half of the centrosymmetric dimer has been de-emphasised.

[61]. The compounds $[RuL_2][PF_6]_2$ (L = **79**, **81**, **87** and **93**) exhibit an electrochemical Ru(II/III) couple between $+0.61 \leq E_{1/2} \leq +0.96$ V versus SCE in CH_2Cl_2, while deprotonation of $[Ru(\mathbf{81})(\mathbf{113})][PF_6]_2$ reduces its oxidation potential from +0.71 V to +0.37 V in the same solvent [61]. $[Ru(\mathbf{81})_2]Cl_2$ has been crystallographically characterised as its hepta-chloroform solvate, and shows the expected six-coordinate structure (Fig. 13) [72]. The complex

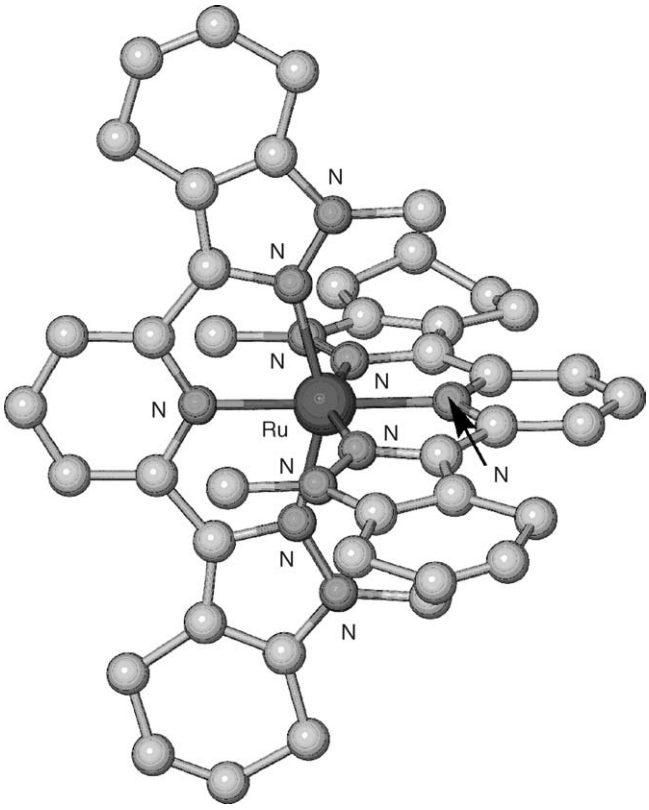

Fig. 13. View of the complex dication in the single crystal structure of $[Ru(\mathbf{81})_2]Cl_2{\cdot}7CHCl_3$ [72]. For clarity, all H atoms have been omitted.

[{Ru(**81**)}$_2$(μ-**128**)][PF$_6$]$_4$ formed in situ upon treatment of [RuCl$_3$(**81**)] with half an equivalent of preformed **128** in ethylene glycol, but could not be isolated in pure form [61]. An attempt to prepare the same compound by reaction of [Ru(**81**)(**113**)][PF$_6$]$_2$ with CH_2Br_2 in the presence of base (cf. the synthesis of **128** [62]) failed. [RuCl$_2$(dmso)(**104**)], [Ru(**104**)$_2$][PF$_6$]$_2$ and [Ru(terpy)(**104**)][PF$_6$]$_2$ were all accessible from **104** and [RuCl$_2$(dmso)$_4$] by the usual procedures [66]. However, similar reactions using **105** gave [RuCl$_2$(dmso)(**105**)] as the only isolable product. The two ferrocenyl moieties in [RuCl$_2$(dmso)(**105**)] were oxidised at the same potential, of $E_{1/2}$ = +0.58 V versus SCE in MeCN [66].

Titration of [Ru(**88**)$_2$][PF$_6$]$_2$ with triethylamine in CD_3CN led to substantial broadening of its ^{1}H NMR spectrum, which was taken as evidence for [HNEt$_3$]$_{2-n}$[Ru(**88**-*n*H)$_2$] (n = 3 or 4) ion pair formation in solution [61]. Performing a similar reaction in the presence of methylviologen dihexafluorophosphate led to precipitation of a salt formulated as [MV^{2+}][Ru(**88**-2H)(**88**-H)]$_2$. In contrast, [Ru(**79**)$_2$][PF$_6$]$_2$ does not interact with NEt_3 by NMR. The compounds [Ru(L″)$_2$][PF$_6$]$_2$ (L″ = **81**, **87** and **88**) have been examined as photosensitisers for oxidation of methylviologen in MeCN [151]. The efficiency of photo-electron transfer from the ruthenium complex to MV^{2+} was more than twice as high for [Ru(**88**)$_2$][PF$_6$]$_2$ as for the other two compounds, which was attributed to supramolecular ion pairing between the MV^{2+} dication and the (deprotonated) complex carboxylate groups as above. The rate of this photoelectron transfer implies that these three compounds have photoexcited state lifetimes of the order of ns at room temperature in solution, and so do not luminesce [151].

4.5. Lanthanide complexes

The compounds [M(**75**)$_3$][PF$_6$]$_3$ (M = Eu, Gd, Tb and Ho) have been synthesised, and three of the four crystallographically characterised [152]. Each of these compounds is isostructural, and shows a tricapped trigonal prismatic coordination geometry (Fig. 14) that is similar to adopted by [Ln(terpy)$_3$]$^{3+}$ complexes [153]. The terbium complex is luminescent, with τ = 1.46 ms in CH_2Cl_2 and 1.09 ms in MeOH. This compound gave a hydration number (q) of 0.6 in MeOH solution, which is consistent with its nine-coordinate geometry being retained in this solvent. A similar experiment in water gave q = 4.6, implying that partial ligand dissociation had taken place [152]. The use of **100** as a lanthanide photosensitiser for biological sensing applications has been described in a patent [63].

5. 2,6-Di(pyrazol-1-yl)pyrazine ligands and their complexes

2,6-Di(pyrazol-1-yl)pyrazines can be synthesised in the same way as their pyridine-containing congeners, by the nucleophilic coupling of 2 equiv. of deprotonated pyrazole with 2,6-dichloropyrazine (Eq. (5)) [25,154,155].

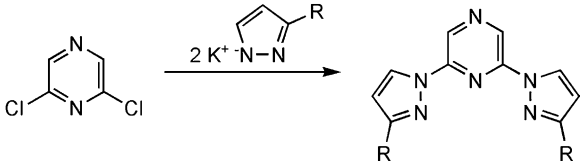

(5)

Ligands **137** [154], **138**, **139** and **146** [155] and **140** [25] have been prepared by this route in purified yields of 30–77%, while elaboration of **140** according to the sequence in Scheme 7 yielded **141**–**145** [25]. The reaction in Eq. (5) is more facile than for the pyridine case (Eq. (1)), being complete after 12–16 h at 90 °C in dmf. For this reason, it is not possible to stop the reaction cleanly half-way to make a chloropyrazine-containing analogue of **I** (Section 2.1), and no asymmetrically substituted 2,6-di(pyrazol-1-yl)pyrazines comparable to **29**–**34** have been made. **147** and **148** were detected as byproducts in the syntheses of **138** and **139**, respectively, but not isolated [155]. The single crystal structure of **137** exhibits an essentially identical molecular conformation to that shown by **1** (Fig. 1, Section 2.1) [154].

The BF_4^- and ClO_4^- salts of [FeL$_2$]$^{2+}$ (L = **137**–**139** and **146**) have been prepared [155]. [Fe(**137**)$_2$]X$_2$ (X = BF_4^- and ClO_4^-) both show abrupt high → low-spin-state transitions upon cooling, with $T_{1/2}$ = 223 and 206 K, respectively. These transitions are identical in form to that shown by [Fe(**1**)$_2$][BF$_4$]$_2$ [75,76] (Section 3.1). Powder diffraction measurements showed that [Fe(**137**)$_2$][ClO$_4$]$_2$ is isostructural with [Fe(**1**)$_2$][BF$_4$]$_2$ at room temperature but, unlike the **1**-containing compound, it undergoes a crystallographic phase change at the spin-crossover temperature [155,156].

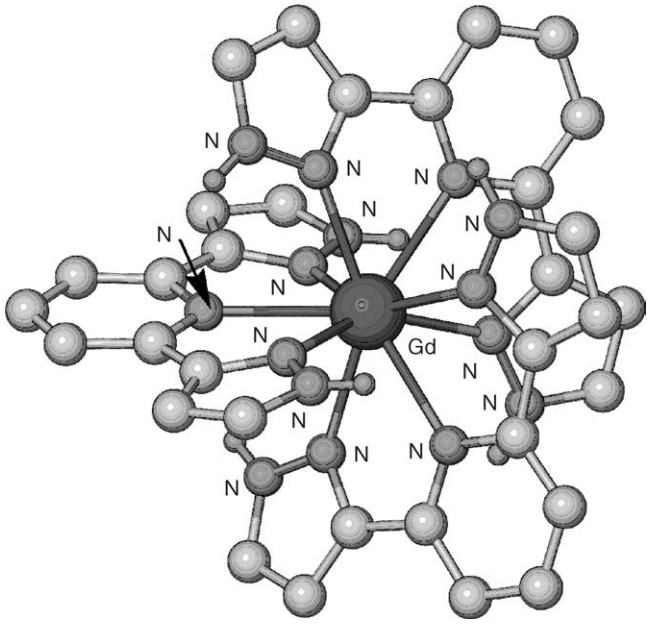

Fig. 14. View of the complex trication in the single crystal structure of [Gd(**75**)$_3$][PF$_6$]$_3$ [152]. For clarity, all C-bound H atoms have been omitted.

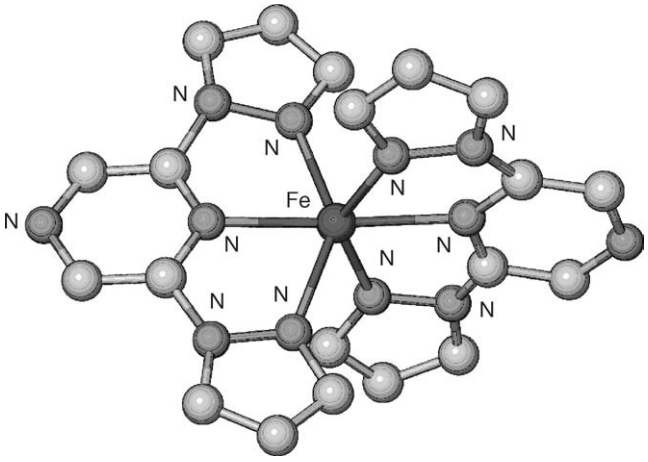

Fig. 15. View of the complex dication in the powder diffraction structure of $[Fe(\mathbf{137})_3][ClO_4]_2$ [156]. For clarity, all H atoms have been omitted.

The unit cell dimensions of the high- and low-temperature phases are similar, except that the *a*-axis length has doubled in the low-temperature phase. A structural refinement of the high-temperature phase was achieved from the powder diffraction data (Fig. 15) [156]. Both these salts undergo a LIESST transition [79] (Section 3.1) to a metastable high-spin state following laser irradiation at 5 K [82]. In contrast to these salts, $[Fe(\mathbf{137})_2][SbF_6]_2$ is fully high-spin between 5 and 300 K, and exhibits a highly twisted six-coordinate coordination geometry analogous to that shown by $[Fe(\mathbf{1})_2][PF_6]_2$ (Section 3.1, Fig. 5) [157]. This is the only known complex of a ligand from the 2,6-dipyrazolylpyrazine series to exhibit this structure.

The thermal spin-crossover transitions in $[Fe(\mathbf{138})_2]X_2$ ($X = BF_4^-$ and ClO_4^-) are discontinuous, involving two discrete steps (Fig. 16) [155]. Unusually for compounds showing such behaviour, crystals of these compounds (which are isostructural) show only a single iron environment in their unit cells [158]. The first, more abrupt part of the transition is initiated by an order:disorder transition of one of the two anion environments in the crystal, which allows an apparently random distribution of half the iron centres in the sample to undergo spin-crossover. The remaining high-spin fraction then undergoes spin-crossover much more gradually as the temperature is decreased further [158]. The two salts of $[Fe(\mathbf{139})_2]^{2+}$ and $[Fe(\mathbf{146})_2]^{2+}$ that were studied were both low-spin at room temperature [155]; for $[Fe(\mathbf{146})_2]^{2+}$, this is a result of intraligand steric interactions between the pyrazole 5-methyl substituent and the pyridine H3 atoms.

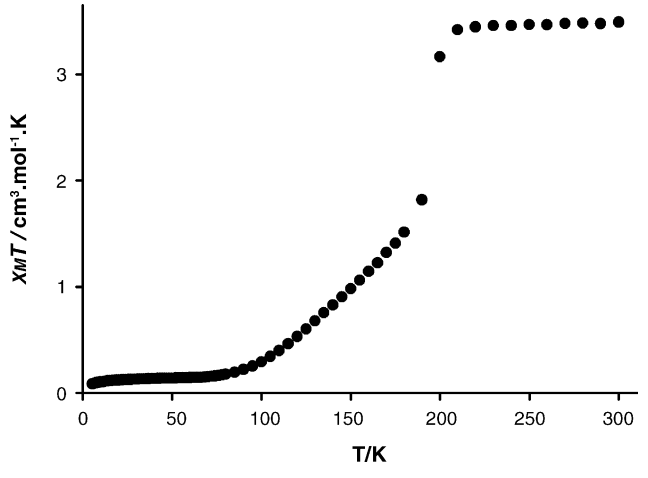

Fig. 16. Susceptibility vs. temperature plot for $[Fe(\mathbf{138})_3][ClO_4]_2$, showing the discontinuous spin-state transition undergone by this compound [155,158].

Complexation of $AgSbF_6$ by 1 equiv. of **137** yields the dinuclear helical compound $[Ag_2(\mu\text{-}\mathbf{137})_2][SbF_6]_2$ [154]. The silver centres in the crystal structure of this compound are linearly coordinated by the ligand pyrazole N-donors only. Attempts to prepare coordination polymers of silver(I) using this ligand, via *N*,*N*′-bridging of the pyrazine ring, were unsuccessful [154]. This correlates with the iron(II) complex chemistry described in the previous paragraphs, where the ligand pyrazine *N*4 atoms showed no tendency to form intermolecular dative-covalent or hydrogen bonds [155]. Presumably, this reflects the reduced basicity of the pyrazine ring in these ligands caused by the two strongly electron-withdrawing pyrazol-1-yl substituents.

Europium(III), terbium(III), dysprosium(III) and samarium(III) complexes of **145** were generated in situ, by mixing equimolar amounts of **145** and the appropriate metal trichloride in aqueous solution [25]. All the resultant solutions show the characteristic lanthanide luminescence [128] upon UV irradiation of a ligand $n \rightarrow \pi^*$ transition [126], which appeared to be unaffected by the fluorescent nature of uncomplexed **145**. The quantum yields obtained from these compounds were comparable to those of lanthanide complexes of **48**, but poorer than those of **15** (Section 3.5) [25,126]. As for **15** and **48**–**52** (Section 3.5), the europium and terbium complexes of **145** gave hydration numbers of 0.3–0.5 [25]. That is, the lanthanide ions are almost perfectly encapsulated by (potentially nonadentate) **145**.

6. 6-Pyrazolyl-2,2′-bipyridines and their complexes

The 6-(pyrazol-1-yl)-2,2′-bipyridine derivatives **149** and **150** have been prepared both by reaction of 6-chloro-2,2′-bipyridine with 1 equiv. of potassium pyrazolide salts (cf. Eq. (1)), and by condensation of 6-hydrazino-2,2′-bipyridine with the appropriate β-diketones (cf. Scheme 3) [159]. The first approach gives the higher yields, of 70-80%, and has also been used to prepare **151** [160]. The compounds **152** and **153** have been described in a patent [161].

The solids $[Fe(\mathbf{149})_2][BF_4]_2{\cdot}H_2O$ and $[Fe(\mathbf{149})_2][ClO_4]_2{\cdot}H_2O$ are fully low-spin at room-temperature [162], while $[Fe(\mathbf{149})_2][PF_6]_2$ [80] and $[Fe(\mathbf{150})_2][PF_6]_2$ [163] are also low-spin in acetone solution. The iron(II/III) redox couples for $[Fe(\mathbf{149})_2]^{2+}$ [80] and $[Fe(\mathbf{150})_2]^{2+}$ [163] are chemically reversible by voltammetry in MeCN. The half-potentials of these oxidations are within

100 mV of each other, with the oxidation potential of $[Fe(terpy)_2]^{2+}$ lying between these two values [163]. In contrast, the cobalt(II/III) oxidation exhibited by $[Co(\mathbf{149})_2]^{2+}$ under the same conditions is 0.34 V less positive than for $[Co(\mathbf{1})_2]^{2+}$, and 0.32 V more positive than for $[Co(terpy)_2]^{2+}$ [80]. The very different behaviour of the iron and cobalt systems reflects the different electron configurations of the two metal ions. Oxidation of (high-spin) cobalt(II) involves loss of an electron from an e_g d-orbital (in O_h symmetry), which is Co–N antibonding and whose energy is therefore very dependent on the σ-basicity of the ligand donors. On the other hand, oxidation of (low-spin) iron(II) results in loss of an electron from a t_{2g} d-orbital, which is non-bonding with respect to the Fe–N σ-bonds. So, the iron(II/III) potentials are insensitive to the different N-donor types in these complexes. The compound $[Ni(\mathbf{149})_2][BF_4]_2$ has also been synthesised [162].

The ruthenium complexes $[RuL_2][PF_6]_2$ (L = **149** and **150**) have been prepared, and show reversible ruthenium(II/III) couples by voltammetry that lie within 100 mV of each other, but are less positive than for both $[Ru(\mathbf{1})_2]^{2+}$ and $[Ru(terpy)_2]^{2+}$ (cf. the iron and cobalt systems in the previous paragraph) [159]. This difference was rationalised by the synergistic metal–ligand π-bonding produced by the *trans*-disposition of π-acceptor pyridine and π-donor pyrazole groups in $[Ru(\mathbf{149})_2]^{2+}$ and $[Ru(\mathbf{150})_2]^{2+}$, which is not present in the other two compounds. That the same trend is not present in the corresponding iron complexes (see above) reflects the reduced π contribution to metal–ligand bonding for a 3d metal compared to a 4d metal.

Treatment of $[ReX(CO)_5]$ ($X = Cl^-$, Br^- or I^-) with (L = **149**–**151**) affords a series of octahedral compounds of structure *fac*-$[ReX(CO)_3L]$ [160]. These compounds contain bidentate **149**–**151** ligands, which are bound to the metal centres through their two pyridyl N-donors only by crystallography (Fig. 17) [164]. The proportion of molecules exhibiting the two possible structures, 'bipyridyl'-coordinated and 'pyrazolylpyridine'-coordinated, is ca. 80:20 in $CDCl_3$ solutions of these compounds at room temperature [160]. The two structures undergo chemical exchange by a concerted 'tick-tock' mechanism (cf. Section 3.4). The compounds $[PtClMe_3(\mathbf{149})]$ and $[PtIMe_3(L)]$ (L = **149**–**151**) have also been prepared [165]. The crystal structure of $[PtIMe_3(\mathbf{150})]$ shows an octahedral platinum(II) centre, bound to a bidentate **150** ligand through its two pyridyl donors as before. This 'bipyridyl-coordinated' structure is the only one detectable by NMR in $CDCl_3$ solution at room temperature, although fluxional migration of the Pt centres between the terminal pyridine and pyrazole functions was detected upon cooling [165].

2-(3,5-Dimethylpyrazol-1-yl)-1,10-phenanthroline (**154**) has been synthesised in ca. 50% yield, from 2-hydrazino-1,10-phenanthroline and 2,4-pentanedione as before [166,167]. Hydrated iodide and nitrate, and anhydrous tetrafluoroborate, salts of $[Fe(\mathbf{154})_2]^{2+}$ all undergo gradual high → low-spin-state transitions upon cooling, that are centred near room temperature in the solid and around 330 K in acetone solution [166]. $[Ni(\mathbf{154})_2][BF_4]_2$ has also been prepared [166].

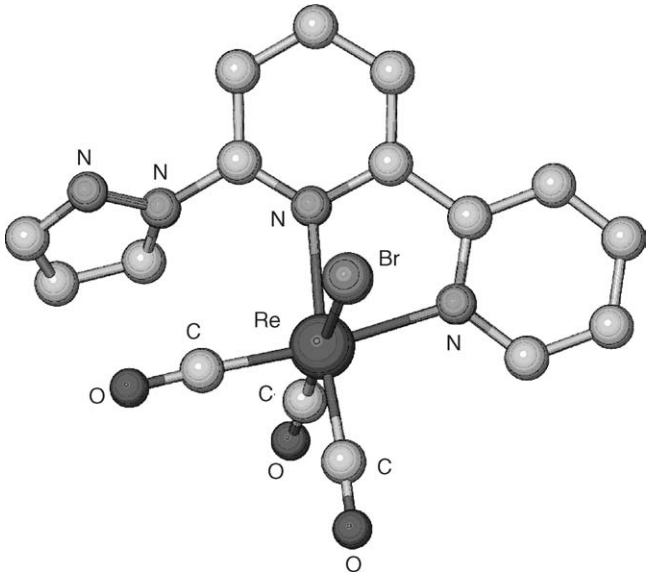

Fig. 17. View of one of the two crystallographically independent molecules in the single crystal structure of $[ReBr(CO)_3(\mathbf{149})]$ [164]. For clarity, all H atoms have been omitted.

A Stille coupling of 1-(6-bromopyrid-2-yl)-4-pyrazolecarbaldehyde and 2-(tributylstannyl)-5-(1,3-dioxolan-2-yl)pyridine yielded **155** after an aqueous acid work-up. This was converted into **156** and **157** in yields of 9–18%, by the same methodology used for **65** and **66** (Section 2.1) [168]. The single crystal X-ray structure of **156** shows near-coplanar, *transoid* pyridine and pyrazole rings, as expected (cf. **1** [49]), but with the nitronylnitroxide groups twisted significantly out of the tris-heterocyclic plane. A variable temperature EPR study of **156** in frozen toluene solution demonstrated ferromagnetic coupling between the two unpaired spins in the molecule, with $2J = 13.3 \pm 4.9\ cm^{-1}$. Comparison of the variable temperature EPR properties of **65**, **156** and an analogous diradical linked containing a 2,2′:6′,2″-terpyrid-5,5′-diyl spacer showed that a pyrazole ring is much less effective than a pyridine ring at mediating ferromagnetic coupling between the radical centres [168].

6-(Pyrazol-3-yl)-2,2′-bipyridine (**158**) has been synthesised in 72–76% yield using the same methodology employed for **75** (Eq. (3)), starting from 6-acetyl-2,2′-bipyridine [169]. Treatment of copper(II) acetate with **158** and NH_4PF_6 yields $[Cu_4(\mu\text{-}\{\mathbf{158}\text{–H}\})_4(dmf)_4][PF_6]_4{\cdot}6dmf$ after recrystallisation from dmf [170]. This complex has an approximately S_4-symmetric cyclic tetranuclear structure, in which the copper(II) ions are bridged by deprotonated **158** pyrazolido functions (Fig. 18). Prolonged drying of this compound in vacuo results in loss of the complete dmf content from the solid, yielding solvent-free $[Cu_4(\mu\text{-}\{\mathbf{158}\text{–H}\})_4][PF_6]_4$. This solvent-free material exhibits antiferromagnetic coupling between the copper centres with $J = 63.5\ cm^{-1}$ [for

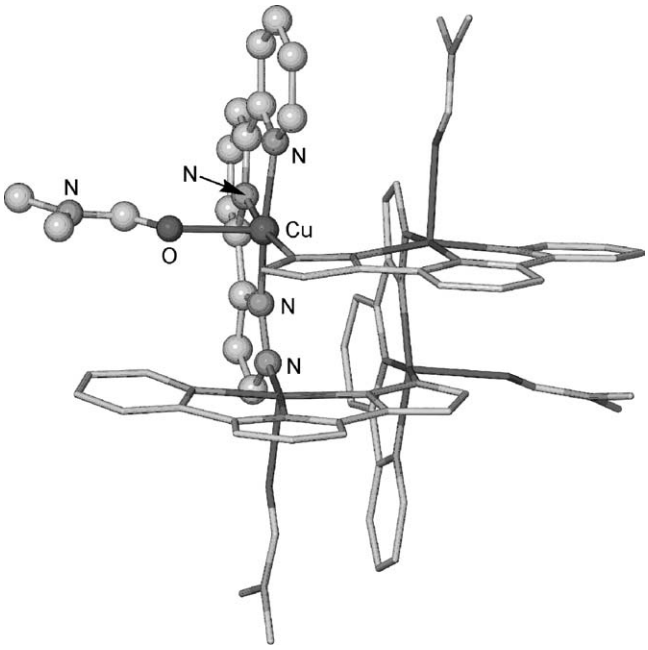

Fig. 18. View of the complex tetracation in the single crystal structure of $[Cu_4(\mu\text{-}\{\mathbf{158}\text{-H}\})_4(dmf)_4][PF_6]_4\cdot 6dmf$ [169]. For clarity, all C-bound H atoms have been omitted and three of the four $[Cu(\mathbf{158}\text{-H})(dmf)]^+$ moieties in the molecule have been de-emphasised.

$H = J\sum(S_1 \cdot S_2)$], and shows a spin-triplet EPR spectrum at 100 K [170]. Reaction of molten **158** with KBH_4 gives a 42% yield of the potassium salt of the bis(pyrazolylborate) derivative **159** [169,171]. **159** forms dinuclear double-helical complexes $[K_2(\mu\text{-}\mathbf{159})_2]$ [169,171] and $[Cu_2(\mu\text{-}\mathbf{159})_2][BF_4]_2$ [169], but mononuclear [Tl(**159**)] [169] and $[M(\mathbf{159})(NO_3)_2]$ (M = Gd or Eu) [169,172] complexes with larger metal ions. In the latter compounds the metal ions are 10-coordinate in the crystal, with two bidentate nitrate ligands.

7. 6,6′-Di(pyrazolyl)-2,2′-bipyridines and their complexes

Reaction of the $Ni[ClO_4]_2$ complex of 6,6′-dihydrazino-2,2′-bipyridine with 2 equiv. of 2,4-pentanedione or benzoylacetone yields nickel-bound **160** and **161**, respectively [173,174]. These ligands were also isolated in metal-free form by treatment of the nickel complexes with NaCN or, for **161** only, by the direct reaction of the same two precursors in the absence of a nickel salt [174]. Yields for all these transformations were ca. 80%. The structure of **161** was assigned as the symmetric 3-methyl-5-phenylpyrazolyl regioisomer shown, on the basis of the ^1H chemical shift of its methyl resonance. The complexes $[NiL][ClO_4]_2\cdot xH_2O$ (L = **160**, $x = 1$; L = **161**, $x = 2$), $[NiCl_2(\mathbf{160})]$ and $[Ni(NCS)_2L]$ (L = **160** and **161**) all contain octahedral nickel centres by spectroscopy [174].

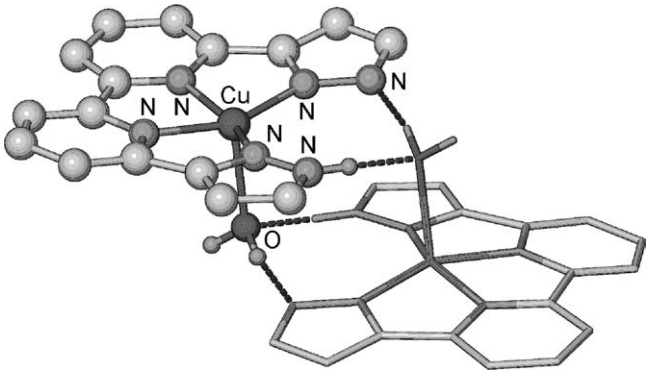

Fig. 19. View of the supramolecular complex dimer dication in the single crystal structure of $[Cu(\mathbf{168}\text{-H})(OH_2)]PF_6$ [175]. For clarity, all C-bound H atoms have been omitted and one half of the centrosymmetric dimer has been de-emphasised.

Compounds **162** [25] and **167** [23] have been prepared in 40–50% yield by a nickel-catalysed coupling reaction (Eq. (6) for **162**).

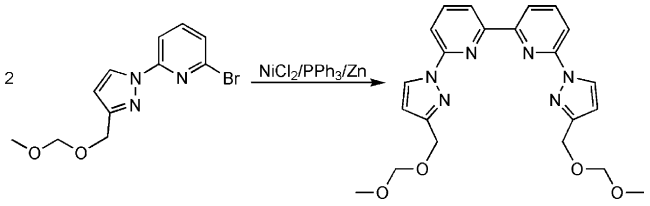

(6)

Deprotection of **162** yields **163**, which was converted sequentially to **164**–**166** by the methods shown in Scheme 7 [25]. The europium(III), terbium(III) samarium(III) and dysprosium(III) complexes of **166** have been prepared and studied in situ in aqueous buffer. The emission lifetime of [Eu(**166**)] is comparable to those of europium complexes of **15**, **48**–**52** and **145** [25,126]. However, [Tb(**166**)] luminesces much less effectively, with a lifetime and quantum yield ten times smaller than the terbium complexes of the other ligands in the previous sentence (cf. Sections 3.5, 4.5 and 5). Apparently, the photoexcited triplet state of the **166** bipyridyl fragment is less well matched to the terbium f-electron energy levels than that of a monopyridyl group contained in this ligand type [25,126].

6,6′-Bis(pyrazol-3-yl)-2,2′-bipyridine (**168**) was synthesised almost quantitatively from 6,6′-diacetyl-2,2′-bipyridine using the same methodology employed for **75** (cf. Eq. (3)), and two of its complexes crystallographically characterised [175]. $Ag_2(\mu\text{-}\mathbf{168})_2][BF_4]_2\cdot H_2O$ is a helical dinuclear complex with flattened tetrahedral silver centres. Mononuclear $[Cu(\mathbf{168}\text{-H})(OH_2)]PF_6$ contains square pyramidal copper(II) centres, which associate into a hydrogen-bonded dimer in the crystal through O–H···N and N–H···O hydrogen bonding between the water ligand on one complex cation and the deprotonated **168** ligand on the other (Fig. 19).

8. Conclusions

The synthetic procedures for both 2,6-di(pyrazolyl)pyridine isomers lend themselves to the introduction of substituents adjacent to the pyrazole N-donor much more easily than at the pyridyl group. Indeed, no 2,6-di(pyrazol-3-yl)pyridines derivatised at the pyridine ring are known. In contrast, most syntheses of terpyridines involve construction of the central pyridine ring, which means that preparation of terpys substituted at the 4′-position is often facile [2]. While several 6,6″-disubstituted terpy ligands have also been reported, their syntheses are rather involved because the required 6-substituted-2-acetylpyridine starting materials are not readily available. From that point of view, the synthetic chemistries of the 2,6-di(pyrazolyl)pyridine and terpy ligand series compliment each other. Obvious examples of this synthetic utility are the lanthanide emission sensitisers shown in Scheme 7, and the different types of macrocyclic ligand structures in this review. No terpyridyl analogues of any of these ligand types have been made.

The terpy and 2,6-di(pyrazolyl)pyridine moieties also differ in the metal-binding characteristics of their respective N-donors. A 'pyridinic' pyrazolyl N atom is much less basic than a pyridyl N donor, as exemplified by the basic pK_as of the parent pyrazole (2.5 [176]) and pyridine (5.23 [177]) heterocycles. The π-bonding capabilities of the two groups are also different, in that conjugated pyridine rings readily accept π-back bonding from a transition ion, while pyrazolyl groups are more π-electron-rich and so are weak π-donors [76,98,178]. The near-identical $T_{1/2}$ values for spin-crossover undergone by $[Fe(\mathbf{1})_2]^{2+}$ (248 K [76]) and $[Fe(\mathbf{75})_2]^{2+}$ (260–270 K [133]) in acetone solution argue that the ligand field exerted by the two 2,6-di(pyrazolyl)pyridine isomers is very similar, and weaker than for terpy (since $[Fe(terpy)_2]^{2+}$ is low-spin [1]). A similar conclusion comes from the substantially greater cobalt(II/III) potential exhibited by $[Co(\mathbf{1})_2]^{2+}$ compared to $[Co(terpy)_2]^{2+}$ [80]. The situation is apparently more complicated in their ruthenium chemistries, however, where metal–ligand π-bonding should be more significant. For example, the ruthenium(II/III) couples shown by the following compounds exhibit the trend: $[Ru(terpy)_2]^{2+}$ (1.27 V versus SCE) ≈ $[Ru(\mathbf{1})_2]^{2+}$ (1.25) > $[Ru(\mathbf{19})_2]^{2+}$ (1.06) > $[Ru(\mathbf{81})_2]^{2+}$ (0.83) > $[Ru(\mathbf{79})_2]^{2+}$ (0.63) [59,108]. This ordering is not easy to explain using simple metal–ligand bonding arguments, and shows that methylation of the 2,6-di(pyrazolyl)pyridine periphery has a substantial effect on the electron-richness of a coordinated ruthenium ion.

Optically pure, chiral versions of both 2,6-di(pyrazolyl)pyridine isomers are readily prepared [20–23,52,57]. However, in contrast to the related 2,6-di(oxazolin-2-yl)pyridine ("PyBox") series of ligands for example [179], there are few reports of the use of 2,6-di(pyrazolyl)pyridine complexes in catalysis [22,57,60,118]. One contributing factor to this might be that sterically hindered 2,6-di(pyrazol-1-yl)pyridines, at least, are prone to dissociate from a coordinated metal ion in solution [101,124,152]. That again reflects the relatively weak donor capabilities of the pyrazolyl groups in these ligands (see above), and would significantly reduce their effectiveness in catalyst systems.

9. Supplementary data

Full crystallographic data for **4** [48] and $[Fe(\mathbf{32})_2][BF_4]_2$ [86], which have not been published elsewhere, are available on request from the Cambridge Crystallographic Data Centre, 12 Union Road, Cambridge CB2 1EZ, UK. The CCDC deposition numbers are 252169 and 252170, respectively.

Acknowledgements

The author's work discussed in this article was carried out by Drs. Nayan Solanki, Joanne Holland and Jérôme Elhaïk, with help from Dr. Victoria Money and Professor Judith Howard FRS (University of Durham) and other collaborators cited in the references. Colin Kilner is acknowledged for the crystal structures of **4** and $[Fe(\mathbf{32})_2][BF_4]_2$. All crystal structure figures in this article were produced with the program EXSEED [180] (which incorporates POVRAY [181]), using coordinates down-loaded from the Cambridge Crystallographic Database [182] where necessary.

References

[1] E.C. Constable, Adv. Inorg. Chem. Radiochem. 30 (1986) 69.
[2] (a) A.M.W. Cargill Thompson, Coord. Chem. Rev. 160 (1997) 1;
(b) R.-A. Fallahpour, Synthesis (2003) 155;
(c) G. Chelucci, R.P. Thummel, Chem. Rev. 102 (2002) 3129.
[3] T.J. Meyer, M.H.V. Huynh, Inorg. Chem. 42 (2003) 8140.
[4] C. Piguet, G. Bernardinelli, G. Hopfgartner, Chem. Rev. 97 (1997) 2005.
[5] (a) J.-P. Sauvage, J.-P. Collin, J.-C. Chambron, S. Guillerez, C. Coudret, V. Balzani, F. Barigelletti, L. De Cola, L. Flamigni, Chem. Rev. 94 (1994) 993;
(b) E. Baranoff, J.-P. Collin, L. Flamigni, J.-P. Sauvage, Chem. Soc. Rev. 33 (2004) 147.
[6] D.R. McMillin, J.J. Moore, Coord. Chem. Rev. 229 (2002) 113.
[7] (a) E.C. Constable, Chem. Commun. (1997) 1073;
(b) A.J. Goshe, J.D. Crowley, B. Bosnich, Helv. Chim. Acta 84 (2001) 2971;
(c) U.S. Schubert, C. Eschbaumer, Angew. Chem. Int. Ed. 41 (2002) 2892;
(d) H. Hofmeier, U.S. Schubert, Chem. Soc. Rev. 33 (2004) 373.
[8] R. Mukherjee, Coord. Chem. Rev. 203 (2000) 151.
[9] D.L. Jameson, K.A. Goldsby, J. Org. Chem. 55 (1990) 4992.
[10] J. Elhaïk, V.A. Money, C.A. Kilner, J.-F. Létard, J.A.K. Howard, M.A. Halcrow, unpublished data.
[11] P. Cornago, C. Escolástico, M.D. Santa María, R.M. Claramunt, C. Fernandez-Castaño, C. Foces-Foces, J.-P. Fayet, J. Elguero, Tetrahedron 52 (1996) 11075.
[12] J.M. Holland, C.A. Kilner, M. Thornton-Pett, M.A. Halcrow, Polyhedron 20 (2001) 2829.
[13] M.A. Halcrow, C.A. Kilner, M. Thornton-Pett, Acta Crystallogr., Sect. C 56 (2000) 213.

[14] C.A. Bessel, R.F. See, D.L. Jameson, M.R. Churchill, K.J. Takeuchi, J. Chem. Soc., Dalton Trans. (1993) 1563.
[15] N.K. Solanki, E.J.L. McInnes, F.E. Mabbs, S. Radojevic, M. McPartlin, N. Feeder, J.E. Davies, M.A. Halcrow, Angew. Chem. Int. Ed. 37 (1998) 2221.
[16] M.J. Remuinan, H. Roman, M.T. Alonso, J.C. Rodríguez-Ubis, J. Chem. Soc., Perkin Trans. 2 (1993) 1099.
[17] E. Brunet, O. Juanes, R. Sedano, J.C. Rodríguez-Ubis, Org. Lett. 4 (2002) 213.
[18] A.-C. Franville, R. Mahiou, D. Zambon, J.-C. Cousseins, Solid State Sci. 3 (2001) 211.
[19] G. Zoppellaro, A. Geies, V. Enkelmann, M. Baumgarten, Eur. J. Org. Chem. (2004) 2367.
[20] A.A. Watson, D.A. House, P.J. Steel, J. Org. Chem. 56 (1991) 4072.
[21] D.D. LeCloux, W.B. Tolman, J. Am. Chem. Soc. 115 (1993) 1153.
[22] D.L. Christenson, C.J. Tokar, W.B. Tolman, Organometallics 14 (1995) 2148.
[23] R. Kowalczyk, J. Skarzewski, Tetrahedron 61 (2005) 623.
[24] N.K. Solanki, M.A. Leech, E.J.L. McInnes, J.P. Zhao, F.E. Mabbs, N. Feeder, J.A.K. Howard, J.E. Davies, J.M. Rawson, M.A. Halcrow, J. Chem. Soc., Dalton Trans. (2001) 2083.
[25] J.C. Rodruígez-Ubis, R. Sedano, G. Barrosso, O. Juanes, E. Brunet, Helv. Chim. Acta 80 (1997) 86 and 80 (1997) 621 (correction).
[26] J. Yuan, G. Wang, K. Majima, K. Matsumoto, Anal. Chem. 73 (2001) 1869.
[27] E. Brunet, O. Juanes, R. Sedano, J.C. Rodruígez-Ubis, Photochem. Photobiol. Sci. 1 (2002) 613.
[28] V.A. Money, J. Elhaïk, M.A. Halcrow, J.A.K. Howard, Dalton Trans. (2004) 1516.
[29] T. Vermonden, D. Branowska, A.T.M. Marcelis, E.J.R. Sudhölter, Tetrahedron 59 (2003) 5039.
[30] (a) R.-A. Fallahpour, Synthesis (2000) 1138;
(b) R.-A. Fallahpour, Synthesis (2000) 1665;
(c) G. Ulrich, S. Bedel, C. Picard, P. Tisnès, Tetrahedron Lett. 42 (2001) 6113.
[31] K. Matsumoto, J. Yuan, G. Wang, M. Tan, PCT Int. WO 2003076938 (2003) 69 pp.
[32] J. Yuan, M. Tan, G. Wang, J. Luminesc. 106 (2004) 91.
[33] (a) I. Singh, A.K. Sharma, S.K. Yadav, D. Singh, S.D. Han, Asian J. Chem. 15 (2003) 185;
(b) I. Singh, A.K. Sharma, D. Singh, S.K. Yadav, Asian J. Chem. 15 (2003) 1069.
[34] S. Checchi, M. Ridi, Gazz. Chim. Ital. 90 (1960) 1093.
[35] (a) R. Fusco, Chem. Heterocycl. Comp. 22 (1967) 3;
(b) G. Coispeau, J. Elguero, Bull. Soc. Chim. Fr. (1970) 2717.
[36] Y. Lin, S.A. Lang Jr., J. Heterocycl. Chem. 14 (1977) 345.
[37] (a) K. Niedenzu, J. Serwatowski, S. Trofimenko, Inorg. Chem. 30 (1991) 524;
(b) J.C. Calabrese, S. Trofimenko, Inorg. Chem. 31 (1992) 4810;
(c) A.L. Rheingold, R.L. Ostrander, B.S. Haggerty, S. Trofimenko, Inorg. Chem. 33 (1994) 3666.
[38] A. Almirante, A. Cerri, G. Fedrizzi, G. Marazzi, M. Santagostino, Tetrahedron Lett. 39 (1998) 3287.
[39] A. Almirante, A. Benicchio, A. Cerri, G. Fedrizzi, G. Marazzi, M. Santagostino, Synlett (1999) 299.
[40] M.R. Grimmett, Adv. Heterocycl. Chem. 57 (1993) 291.
[41] J. Elguero, in: I. Shinkai (Ed.), Comprehensive Heterocyclic Chemistry II, vol. 3, Elsevier, Oxford, UK, 1996, pp. 1–75.
[42] M.R. Grimmett, B. Iddon, Heterocycles 37 (1994) 2087.
[43] A.R. Katritzky, P. Lue, K. Akutagawa, Tetrahedron 45 (1989) 4253.
[44] C. Riemer, E. Borroni, B. Levet-Trafit, J.R. Martin, S. Poli, R.H.P. Porter, M. Bös, J. Med. Chem. 46 (2003) 1273.
[45] (a) R.F. Evans, M. van Ammers, H.J. den Hertog, Recl. Trav. Chim. Pays-Bas 77 (1958) 340;
(b) M. van Ammers, H.J. den Hertog, Recl. Trav. Chim. Pays-Bas 78 (1959) 408.
[46] H. Takalo, V.-M. Mukkala, L. Meriö, J.-C. Rodríguez-Ubis, R. Sedano, O. Juanes, E. Brunet, Helv. Chim. Acta 80 (1997) 372.
[47] K. Matsumoto, K. Majima, T. Fukui, S. Sueda, J. Yuan, RIKEN Rev. 35 (2001) 105.
[48] J. Azéma, C. Galaup, C. Picard, P. Tisnès, P. Ramos, O. Juanes, J.C. Rodríguez-Ubis, E. Brunet, Tetrahedron 56 (2000) 2673.
[49] C.A. Bessel, R.F. See, D.L. Jameson, M.R. Churchill, K.J. Takeuchi, J. Chem. Soc., Dalton Trans. (1992) 3223.
[50] Crystal data for **4**: $C_{19}H_{25}N_5$, M_r 323.44, orthorhombic, *Pbcn*, $a = 16.7209(11)$, $b = 11.8780(6)$, $c = 9.3898(4)$ Å, $V = 1864.92(17)$ Å^3, $Z = 4$, μ(Mo Kα) = 0.071 mm^{-1}, $T = 150(2)$ K, 10995 reflections collected, 1705 unique ($R_{int} = 0.126$), $R_1(F) = 0.063$, $wR_2(F^2) = 0.154$, $S = 1.096$. The asymmetric unit contains half a molecule, with the crystallographic C_2 axis [0, *y*, 1/4] bisecting the pyridine ring.
[51] F. Calderazzo, U. Englert, C. Hu, F. Marchetti, G. Pampaloni, V. Passarelli, A. Romano, R. Santi, Inorg. Chim. Acta 344 (2003) 197.
[52] H. Brunner, T. Scheck, Chem. Ber. 125 (1992) 701.
[53] A.-K. Pleier, H. Glas, M. Grosche, P. Sirsch, W.R. Thiel, Synthesis (2001) 55.
[54] M. Gal, G. Tarrago, P. Steel, C. Marzin, New J. Chem. 9 (1985) 617.
[55] T. Zhou, B. Pesic, Hydrometallurgy 46 (1997) 37.
[56] R. Dash, P. Potvin, Can. J. Chem. 70 (1992) 2249.
[57] C. Kashima, S. Shibata, H. Yokoyama, T. Nishio, J. Heterocycl. Chem. 40 (2003) 773.
[58] P. van der Valk, P.G. Potvin, J. Org. Chem. 59 (1994) 1766.
[59] J. Zadykowicz, P.G. Potvin, Inorg. Chem. 38 (1999) 2434.
[60] R. Jairam, M.L. Lau, J. Adorante, P.G. Potvin, J. Inorg. Biochem. 84 (2001) 113.
[61] J. Zadykowicz, P.G. Potvin, Inorg. Chem. 38 (1999) 2434.
[62] J. Zadykowicz, P.G. Potvin, J. Org. Chem. 63 (1998) 235.
[63] H. Takalo, V.M. Mukkala, PCT Int. Appl. WO 9311433 A1 19930610 (1993) 78 pp.
[64] G. Dong, A.T. Baker, D.C. Craig, Inorg. Chim. Acta 231 (1995) 241.
[65] A.T. Baker, D.C. Craig, G. Dong, Inorg. Chem. 35 (1996) 1091.
[66] N. Chabert-Couchouron, C. Marzin, G. Tarrago, New J. Chem. 21 (1997) 355.
[67] J. Chin, S. J. Lee, S.J. West, PCT Int. WO 2002071057 A1 20020912 (2002) 31 pp.
[68] J. Zadykowicz, P.G. Potvin, J. Heterocycl. Chem. 36 (1999) 623.
[69] F. Al-Omran, N. Al-Awadi, M. Edun, J. Chem. Res. (S) (1994) 168;
F. Al-Omran, N. Al-Awadi, M. Edun, J. Chem. Res. (M) (1994) 1026.
[70] V.I. Minkin, A.D. Garnovskii, J. Elguero, A.R. Katritzky, O.V. Denisko, Adv. Heterocycl. Chem. 76 (2000) 157.
[71] K.H. Sugiyarto, M.L. Scudder, D.C. Craig, H.A. Goodwin, Aust. J. Chem. 53 (2000) 755.
[72] J. Zadykowicz, P.G. Potvin, J. Coord. Chem. 47 (1999) 395.
[73] (a) F. Aguilar-Parrilla, G. Scherer, H.H. Limbach, M.C. Foces-Foces, F.H. Cano, J.A.S. Smith, C. Toiron, J. Elguero, J. Am. Chem. Soc. 114 (1992) 9657;
(b) C. Foces-Foces, A.L. Llamas-Saiz, R.M. Claramunt, C. López, J. Elguero, J. Chem. Soc., Chem. Commun. (1994) 1143;
(c) F. Aguilar-Parrilla, H.-H. Limbach, C. Foces-Foces, F.H. Cano, N. Jagerovic, J. Elguero, J. Org. Chem. 60 (1995) 1965;
(d) M.A. Halcrow, H.R. Powell, M.J. Duer, Acta Crystallogr., Sect. B 52 (1996) 746.
[74] C. Lopez, R.M. Claramunt, S. Trofimenko, J. Elguero, Can. J. Chem. 71 (1993) 678.

[75] J.M. Holland, J.A. McAllister, Z. Lu, C.A. Kilner, M. Thornton-Pett, M.A. Halcrow, Chem. Commun. (2001) 577.
[76] J.M. Holland, J.A. McAllister, C.A. Kilner, M. Thornton-Pett, A.J. Bridgeman, M.A. Halcrow, J. Chem. Soc., Dalton Trans. (2002) 548.
[77] E.C. Constable, G. Baum, E. Bill, R. Dyson, R. van Eldik, D. Fenske, S. Kaderli, D. Morris, A. Neubrand, M. Neuberger, D.R. Smith, K. Wieghardt, M. Zehnder, A.D. Zuberbühler, Chem. Eur. J. 5 (1999) 498.
[78] J. Elhaïk, D.J. Evans, C.A. Kilner, M.A. Halcrow, Dalton Trans., in press.
[79] M.B. Darkhovskii, A.L. Tchougreeff, J. Phys. Chem. A 108 (2004) 6351.
[80] T. Ayers, S. Scott, J. Goins, N. Caylor, D. Hathcock, S.J. Slattery, D.L. Jameson, Inorg. Chim. Acta 307 (2000) 7.
[81] P. Gütlich, Y. Garcia, H.A. Goodwin, Chem. Soc. Rev. 29 (2000) 419.
[82] V.A. Money, J.S. Costa, S. Marcén, G. Chastanet, J. Elhaïk, M.A. Halcrow, J.A.K. Howard, J.-F. Létard, Chem. Phys. Lett. 391 (2004) 273.
[83] V.A. Money, I. Radosavljevic Evans, M.A. Halcrow, A.E. Goeta, J.A.K. Howard, Chem. Commun. (2003) 158.
[84] (a) J. Kusz, H. Spiering, P. Gütlich, J. Appl. Cryst. 34 (2001) 229; (b) M. Marchivie, P. Guionneau, J.A.K. Howard, A.E. Goeta, G. Chastanet, J.-F. Létard, D. Chasseau, J. Am. Chem. Soc. 124 (2002) 194; (c) E.J. MacLean, C.M. McGrath, C.J. O'Conner, C. Sangregorio, J.M.W. Seddon, E. Sinn, F.E. Sowrey, S.J. Teat, A.E. Terry, G.B.M. Vaughan, N.A. Young, Chem. Eur. J. 9 (2003) 5314; (d) A.L. Thompson, A.E. Goeta, J.A. Real, A. Galet, M.C. Muñoz, Chem. Commun. (2004) 1390; (e) N. Huby, L. Guérin, E. Collet, L. Toupet, J.-C. Ameline, H. Cailleau, T. Roisnel, T. Tayagaki, T. Tanaka, Phys. Rev. B 69 (2004) 20101.
[85] M.L. Scudder, H.A. Goodwin, I.G. Dance, New J. Chem. 23 (1999) 695.
[86] J.M. Holland, S.A. Barrett, C.A. Kilner, M.A. Halcrow, Inorg. Chem. Commun. 5 (2002) 328.
[87] F. Pelascini, M. Wesolek, F. Peruch, A. De Cian, N. Kyritsakas, P.J. Lutz, J. Kress, Polyhedron 23 (2004) 3193.
[88] Crystal data for $[Fe(\mathbf{32})_2][BF_4]_2$: $C_{26}H_{26}B_2F_8FeN_{10}$, M_r 708.04, monoclinic, $P21/n$, $a = 8.2464(1)$, $b = 38.4863(5)$, $c = 9.2506(2)$ Å, $\beta = 96.9154(7)^\circ$, $V = 2914.54(8)$ Å^3, $Z = 4$, μ(Mo Kα) = 0.607 mm^{-1}, $T = 150(2)$ K, 16843 reflections collected, 6409 unique ($R_{int} = 0.063$), $R_1(F) = 0.041$, $wR_2(F^2) = 0.102$, $S = 1.030$.
[89] J. Elhaïk, C.A. Kilner, M.A. Halcrow, Cryst. Eng. Comm. 7 (2005) 151.
[90] M.A. Halcrow, C.A. Kilner, Acta Cryst. C59 (2003) m61.
[91] C. Arici, D. Ülkü, R. Kurturan, K.C. Emregül, O. Atakol, Z. Kristallogr. 218 (2003) 497.
[92] R. Kurtaran, C. Arici, K.C. Emregül, D. Ülkü, O. Atakol, M. Taştekin, Z. Anorg. Allg. Chem. 629 (2003) 1617.
[93] M.A. Leech, N.K. Solanki, M.A. Halcrow, J.A.K. Howard, S. Dahaoui, Chem. Commun. (1999) 2245.
[94] N.K. Solanki, M.A. Leech, E.J.L. McInnes, F.E. Mabbs, J.A.K. Howard, C.A. Kilner, J.M. Rawson, M.A. Halcrow, J. Chem. Soc., Dalton Trans. (2002) 1295.
[95] G.S. Beddard, M.A. Halcrow, M.A. Hitchman, M.P. de Miranda, C.J. Simmons, H. Stratemeier, Dalton Trans. (2003) 1028.
[96] I.B. Bersuker, The Jahn–Teller Effect and Vibronic Interactions in Modern Chemistry, Plenum, New York, 1984.
[97] M.A. Halcrow, Dalton Trans. (2003) 4375.
[98] A.J. Bridgeman, M.A. Halcrow, M. Jones, E. Krausz, N.K. Solanki, Chem. Phys. Lett. 314 (1999) 176.
[99] J.M. Holland, X. Liu, J.P. Zhao, F.E. Mabbs, C.A. Kilner, M. Thornton-Pett, M.A. Halcrow, J. Chem. Soc., Dalton Trans. (2000) 3316.
[100] M.A. Halcrow, C.A. Kilner, J. Wolowska, E.J.L. McInnes, A.J. Bridgeman, New J. Chem. 28 (2004) 228 and 28 (2004) 887 (correction).
[101] N.K. Solanki, E.J.L. McInnes, D. Collison, C.A. Kilner, J.E. Davies, M.A. Halcrow, J. Chem. Soc., Dalton Trans. (2002) 1625.
[102] S. Chakrabarty, R.K. Poddar, R.D. Poulsen, A.L. Thompson, J.A.K. Howard, Acta Cryst. C60 (2004) 628.
[103] A.J. Blake, S.J. Hill, P.J. Hubberstey, Chem. Commun. (1998) 1587.
[104] R. Kurtaran, C. Arici, S. Durmu, D. Ülkü, O. Atakol, Anal. Sci. 19 (2003) 335.
[105] G. Baum, A.J. Blake, D. Fenske, P. Hubberstey, C. Julio, M.A. Withersby, Acta Cryst. C58 (2002) 542.
[106] N.K. Solanki, A.E.H. Wheatley, S. Radojevic, M. McPartlin, M.A. Halcrow, J. Chem. Soc., Dalton Trans. (1999) 521.
[107] M.A. Halcrow, C.A. Kilner, M. Thornton-Pett, Acta Cryst. C56 (2000) 1425.
[108] D.L. Jameson, J.K. Blaho, K.T. Kruger, K.A. Goldsby, Inorg. Chem. 28 (1989) 4312.
[109] S.A. Willison, H. Jude, R.M. Antonelli, J.M. Rennekamp, N.A. Eckert, K.A. Krause Bauer, W.B. Connick, Inorg. Chem. 43 (2004) 2548.
[110] A.C. Laemmel, J.-P. Collin, J.-P. Sauvage, C. R. Acad. Sci. Paris, Ser. IIc 3 (2000) 34.
[111] C.A. Bessel, R.F. See, D.L. Jameson, M.R. Churchill, K.J. Takeuchi, J. Chem. Soc., Dalton Trans. (1991) 2801.
[112] R.A. Leising, S.A. Kubow, M.R. Churchill, L.A. Buttrey, J.W. Ziller, K.J. Takeuchi, Inorg. Chem. 29 (1990) 1306.
[113] N.J. Beach, G.J. Spivak, Inorg. Chim. Acta 343 (2003) 244.
[114] S.J. Slattery, W.D. Bare, D.L. Jameson, K.A. Goldsby, J. Chem. Soc., Dalton Trans. (1999) 1347.
[115] V.J. Catalano, R. Kyrtaran, R.A. Heck, A. Öhman, M.G. Hill, Inorg. Chim. Acta 286 (1999) 181.
[116] B.A. Moyer, M.S. Thompson, T.J. Meyer, J. Am. Chem. Soc. 102 (1980) 2310.
[117] W.-H. Fung, W.-C. Cheng, W.-Y. Yu, C.-M. Che, T.C.W. Mak, J. Chem. Soc., Chem. Commun. (1995) 2007.
[118] W.-H. Fung, W.-Y. Yu, C.-M. Che, J. Org. Chem. 63 (1998) 7715.
[119] K. Chryssou, V.J. Catalano, R. Kurtaran, P. Falaras, Inorg. Chim. Acta 328 (2002) 204.
[120] K. Chryssou, T. Stergiopoulos, P. Falaras, Polyhedron 21 (2002) 2773.
[121] (a) P. Falaras, K. Chryssou, T. Stergiopoulos, I. Arabatzis, G. Katsaros, V.J. Catalano, R. Kurtaran, A. Hugot-Le Goff, M.-C. Bernard, Proc. SPIE 4801 (2003) 125; (b) T. Stergiopoulos, S. Karakostas, P. Falaras, J. Photochem. Photobiol. A 163 (2004) 331.
[122] T. Stergiopoulos, M.-C. Bernard, A. Hugot-Le Goff, P. Falaras, Coord. Chem. Rev. 248 (2004) 1407.
[123] E.W. Abel, K.A. Hylands, M.D. Olsen, K.G. Orrell, A.G. Osbourne, V. Šik, G.N. Ward, J. Chem. Soc., Dalton Trans. (1994) 1079.
[124] R.E. Rülke, V.E. Kaasjager, D. Kliphuis, C.J. Elsevier, P.W.N.M. Van Leeuwen, K. Vrieze, K. Koubitz, Organometallics 15 (1996) 668.
[125] F. Ercan, C. Arici, D. Ülkü, R. Kurtaran, M. Aksu, O. Atakol, Z. Kristallogr. 219 (2004) 295.
[126] M. Latva, H. Takalo, V.-M. Mukkala, C. Matachescu, J.C. Rodruígez-Ubis, J. Kankare, J. Luminesc. 75 (1997) 149.
[127] H. Hakala, P. Liitti, K. Puukka, J. Peuralahti, K. Loman, J. Karvinen, P. Ollikka, A. Ylikoski, V.-M. Mukkala, J. Hovinen, Inorg. Chem. Commun. 5 (2002) 1059.
[128] N. Sabbatini, M. Guardigli, J.-M. Lehn, Coord. Chem. Rev. 123 (1993) 201.
[129] S. Sueda, J. Yuan, K. Matsumoto, Bioconjugate Chem. 13 (2002) 200.
[130] Z. Ye, M. Tan, G. Wang, J. Yuan, Anal. Chem. 76 (2004) 513.
[131] Z. Ye, M. Tan, G. Wang, J. Yuan, Talanta 65 (2005) 206.

[132] J.C. Rodriguez-Ubis, H. Takalo, V.-M. Mukkala, Eur. Pat. EP 19970502 (1997) 33 pp.
[133] K.H. Sugiyarto, D.C. Craig, A.D. Rae, H.A. Goodwin, Aust. J. Chem. 47 (1994) 869.
[134] K.H. Sugiyarto, H.A. Goodwin, Aust. J. Chem. 41 (1988) 1645.
[135] H.A. Goodwin, K.H. Sugiyarto, Chem. Phys. Lett. 139 (1987) 470.
[136] T. Buchen, P. Gütlich, H.A. Goodwin, Inorg. Chem. 33 (1994) 4573.
[137] R. Lubbers, G. Nowitzke, H.A. Goodwin, G. Wortmann, J. Phys. IV 7 (1997) 651.
[138] K.H. Sugiyarto, K. Weitzner, D.C. Craig, H.A. Goodwin, Aust. J. Chem. 50 (1997) 869.
[139] T. Buchen, P. Gütlich, K.H. Sugiyarto, H.A. Goodwin, Chem. Eur. J. 2 (1996) 1134.
[140] K.H. Sugiyarto, M.L. Scudder, D.C. Craig, H.A. Goodwin, Aust. J. Chem. 53 (2000) 755.
[141] A. Bhattacharjee, V. Ksenofontov, K.H. Sugiyarto, H.A. Goodwin, P. Gütlich, Adv. Funct. Mater 13 (2003) 877.
[142] K.H. Sugiyarto, W.-A. McHale, D.C. Craig, A.D. Rae, M.L. Scudder, H.A. Goodwin, Dalton Trans. (2003) 2443.
[143] E. Coronado, M.C. Giménez-López, C. Gimenez-Saiz, J.M. Martínez-Agudo, F.M. Romero, Polyhedron 22 (2003) 2375.
[144] H. Paulsen, L. Duelund, H. Winkler, H. Toftlund, A.X. Trautwein, Inorg. Chem. 40 (2001) 2201.
[145] S. Marcén, L. Lecren, L. Capes, H.A. Goodwin, J.-F. Létard, Chem. Phys. Lett. 358 (2002) 87.
[146] R.C.W. Sung, B.R. McGarvey, Inorg. Chem. 38 (1999) 3644.
[147] (a) J.-F. Létard, L. Capes, G. Chastanet, N. Moliner, S. Létard, J.A. Real, O. Kahn, Chem. Phys. Lett. 313 (1999) 115;
(b) N. Shinamoto, S. Ohkoshi, O. Sato, K. Hashimoto, Inorg. Chem. 41 (2002) 678.
[148] P. Gamez, R.H. Steensma, W.L. Driessen, J. Reedijk, Inorg. Chim. Acta 333 (2002) 51.
[149] G. Dong, K.P. Matthews, A.T. Baker, D.C. Craig, Inorg. Chim. Acta 284 (1999) 266.
[150] A.W. Addison, T.N. Rao, J. Reedijk, J. van Rijn, G.C. Verschoor, J. Chem. Soc., Dalton Trans. (1984) 1349.
[151] P.G. Potvin, P.U. Luyen, J. Bräckow, J. Am. Chem. Soc. 125 (2003) 4894.
[152] D.A. Bardwell, J.C. Jeffrey, P.L. Jones, J.A. McCleverty, E. Psillakis, Z. Reeves, M.D. Ward, J. Chem. Soc., Dalton Trans. (1997) 2079.
[153] (a) C. Mallet, R.P. Thummel, C. Hery, Inorg. Chim. Acta 210 (1993) 223;
(b) L.I. Semenova, A.N. Sobolev, B.W. Skelton, A.H. White, Aust. J. Chem. 52 (1999) 519;
(c) J.-C. Berthet, Y. Miquel, P.B. Iveson, M. Nierlich, P. Thuery, C. Madic, M. Ephritikhine, J. Chem. Soc., Dalton Trans. (2002) 3265.
[154] M. Loï, M.W. Hosseini, A. Jouaiti, A. De Cian, J. Fischer, Eur. J. Inorg. Chem. (1999) 1981.
[155] J. Elhaïk, V.A. Money, S.A. Barrett, C.A. Kilner, I. Radosavljevic Evans, M.A. Halcrow, Dalton Trans. (2003) 2053.
[156] V.A. Money, I. Radosavljevic Evans, J. Elhaïk, M.A. Halcrow, J.A.K. Howard, Acta Cryst. B60 (2004) 41.
[157] C.A. Kilner, S.A. Barrett, M.A. Halcrow, Polyhedron, submitted for publication.
[158] V.A. Money, J. Elhaïk, I. Radosavljevic Evans, M.A. Halcrow, J.A.K. Howard, Dalton Trans. (2004) 65.
[159] A.J. Downard, G.E. Honey, P.J. Steel, Inorg. Chem. 30 (1991) 3733.
[160] A. Gelling, K.G. Orrell, A.G. Osbourne, V. Sik, J. Chem. Soc., Dalton Trans. (1994) 3545.
[161] S.F. Sneddon, J.L. Kane, B.H. Hirth, F. Vinick, S. Qiao, S.R. Nahill, PCT Int. WO 2001087849 A2 20011122 (2001) 108 pp.
[162] A.T. Baker, J.P. Matthews, Aust. J. Chem. 52 (1999) 339.
[163] T. Ayers, R. Turk, C. Lane, J. Goins, D. Jameson, S.J. Slattery, Inorg. Chim. Acta 357 (2004) 202.
[164] A. Gelling, K.G. Orrell, A.G. Osborne, V. Sik, M.B. Hursthouse, S.J. Coles, J. Chem. Soc., Dalton Trans. (1996) 203.
[165] A. Gelling, K.G. Orrell, A.G. Osborne, V. Sik, M.B. Hursthouse, S.J. Coles, Polyhedron 15 (1996) 3203.
[166] A.S. Abushamleh, H.A. Goodwin, Aust. J. Chem. 41 (1988) 873.
[167] A.M.S. Garas, R.S. Vagg, J. Heterocycl. Chem. 37 (2000) 151.
[168] G. Zoppellaro, V. Enkelmann, A. Geies, M. Baumgarten, Org. Lett. 6 (2004) 4929.
[169] J.S. Fleming, E. Psillakis, S.M. Couchman, J.C. Jeffery, J.A. McCleverty, M.D. Ward, J. Chem. Soc., Dalton Trans. (1998) 537.
[170] (a) J.C. Jeffery, P.L. Jones, K.L.V. Mann, E. Psillakis, J.A. McCleverty, M.D. Ward, C.M. White, Chem. Commun. (1997) 175;
(b) K.L.V. Mann, E. Psillakis, J.C. Jeffery, L.H. Rees, N.M. Harden, J.A. McCleverty, M.D. Ward, D. Gatteschi, F. Totti, F.E. Mabbs, E.J.L. McInnes, P.C. Riedi, G.M. Smith, J. Chem. Soc., Dalton Trans. (1999) 339.
[171] E. Psillakis, J.C. Jeffery, J.A. McCleverty, M.D. Ward, Chem. Commun. (1997) 479.
[172] N. Armaroli, G. Accorsi, F. Barigelletti, S.M. Couchman, J.S. Fleming, N.C. Harden, J.C. Jeffery, K.L.V. Mann, J.A. McCleverty, L.H. Rees, S.R. Starling, M.D. Ward, Inorg. Chem. 38 (1999) 5769.
[173] J. Lewis, K.P. Wainwright, J. Chem. Soc., Chem. Commun. (1974) 169.
[174] J. Lewis, K.P. Wainwright, J. Chem. Soc., Dalton Trans. (1978) 440.
[175] S.M. Couchman, J.C. Jeffrey, M.D. Ward, Polyhedron 18 (1999) 2633.
[176] J. Elguero, E. Gonzalez, R. Jacquier, Bull. Soc. Chim. Fr. (1968) 5009.
[177] A. Albert, R. Goldacre, J. Phillips, J. Chem. Soc. (1948) 2240.
[178] (a) T. Astley, A.J. Canty, M.A. Hitchman, G.L. Rowbottom, B.W. Skelton, A.H. White, J. Chem. Soc., Dalton Trans. (1991) 1981;
(b) T. Astley, J.M. Gulbis, M.A. Hitchman, E.R.T. Tiekink, J. Chem. Soc., Dalton Trans. (1993) 509.
[179] (a) J.S. Johnson, D.A. Evans, Acc. Chem. Res. 33 (2000) 325;
(b) G. Desimoni, G. Faita, P. Quadrelli, Chem. Rev. 103 (2003) 3119.
[180] L.J. Barbour, J. Supramol. Chem. 1 (2003) 189.
[181] POVRAY v. 3.5, Persistence of Vision Raytracer Pty. Ltd., Williamstown, Victoria, Australia (2002). http://www.povray.org.
[182] F.H. Allen, Acta Cryst. B58 (2002) 380.